

This is an Open Access document downloaded from ORCA, Cardiff University's institutional repository: <https://orca.cardiff.ac.uk/id/eprint/126956/>

This is the author's version of a work that was submitted to / accepted for publication.

Citation for final published version:

Chen, Qing, Zhu, Jianrong, Lyu, Hanghang, Pan, Shunqi and Chen, Shenliang 2019. Impacts of topography change on saltwater intrusion over the past decade in the Changjiang Estuary. *Estuarine, Coastal and Shelf Science* 231 , 106469. 10.1016/j.ecss.2019.106469

Publishers page: <http://dx.doi.org/10.1016/j.ecss.2019.106469>

Please note:

Changes made as a result of publishing processes such as copy-editing, formatting and page numbers may not be reflected in this version. For the definitive version of this publication, please refer to the published source. You are advised to consult the publisher's version if you wish to cite this paper.

This version is being made available in accordance with publisher policies. See <http://orca.cf.ac.uk/policies.html> for usage policies. Copyright and moral rights for publications made available in ORCA are retained by the copyright holders.



1 **Impacts of topography change on saltwater intrusion over the past**  
2 **decade in the Changjiang Estuary**

3  
4  
5 Qing Chen<sup>a,c</sup>, Jianrong Zhu<sup>a,b,\*</sup>, Hanghang Lyu<sup>a</sup>, Shunqi Pan<sup>c</sup>, Shenliang Chen<sup>a,b</sup>

6  
7 <sup>a</sup> State Key Laboratory of Estuarine and Coastal Research, East China Normal University,  
8 Shanghai, 200062, PR China

9 <sup>b</sup> Shanghai Institute of Eco-Chongming, Shanghai, 200062, PR China

10 <sup>c</sup> Hydro-environmental Research Centre, School of Engineering, Cardiff University, Cardiff  
11 CF24 3AA, UK

12  
13  
14  
15 Correspondence should be addressed to Jianrong Zhu

16 E-mail address: jrzh@sklec.ecnu.edu.cn  
17  
18  
19  
20  
21

## 22 **Abstract**

23         Saltwater intrusion in estuaries is mainly controlled by tides and river discharge, as well as  
24 by topography and other factors. The Changjiang estuary has been seen a significant change in  
25 its topography from the data obtained in 2007 and 2017. In this study, a well-validated 3D  
26 numerical model was used to simulate and analyze the residual water and salt transport, water  
27 diversion ratio (WDR) in bifurcated channels and water resources in the Changjiang Estuary in  
28 2007 and 2017. The comparisons of the model results showed that due to the North Branch  
29 becoming much shallower and narrower over the period from 2007 to 2017, the overall salinity  
30 in the North Branch decreased and the intensity of saltwater spillover (SSO) from the North  
31 Branch into the South Branch weakened. In the North Channel, the simulated residual or net  
32 transection water flux (NTWF) and WDR decreased during spring tides, resulting in increased  
33 saltwater intrusion. During neap tides, the saltwater intrusion was weakened despite the  
34 decreased NTWF and WDR because the water depth at the river mouth became shallower. The  
35 changes of topography during that period also resulted in changes of DWR, NTWF, salt  
36 transport across the tidal flats and dykes in the North Passage, South Passage and the South  
37 Channel, as well as overall dynamic mechanism. The results indicated that the salinity at the  
38 water intakes of the three reservoirs in the estuary slightly decreased, indicating that the time  
39 that reservoirs can take water from the estuary become longer in dry seasons. In the scenario of  
40 complete silt-up of the North Branch, the saltwater intrusion was weakened in the South Branch  
41 because of the disappearance of the SSO, which was favorable for the utilization of freshwater  
42 resources, but enhanced in the North Channel, North and South Passages. The overall influence  
43 from the topographic change over the period is that the saltwater intrusion is weakened in the  
44 North Branch, and enhanced during spring tides and weakened during neap tides in the North

45 Channel, North and South Passages. Sediment accretion in the North Branch is favorable for  
46 utilization of freshwater resources.

47

48 **Keywords:** topography change; saltwater intrusion; freshwater resource; numerical model;  
49 Changjiang Estuary.

50

## 51 **1. Introduction**

52 Saltwater intrusion is a common phenomenon in estuaries where freshwater and saltwater  
53 converge. Saltwater intrusion can produce estuarine circulation (Pritchard, 1956) and affect  
54 stratification (Simpson et al., 1990), thereby influencing sediment transport, producing peak  
55 estuarine turbidities (Geyer, 1993), and degrading freshwater quality (Zhu et al., 2010).  
56 Estuarine saltwater intrusion is mainly controlled by tide and river runoff (Pritchard, 1956;  
57 Prandle, 1985; Shen et al., 2003), but it can also be affected by topography (Prandle, 2006),  
58 wind stress (Hansen and Rattray, 1966; Li et al., 2012), and vertical mixing (Ippen and  
59 Harleman, 1961; Simpson and Hunter, 1974; Prandle and Lane, 2015). Prandle (2006)  
60 presented the relation between the estuarine morphological development and the forcing  
61 parameters such as tide range and river flow with the data from 80 UK estuaries. It can be well  
62 explained from these theoretically derived relationships and indicated that estuarine topography  
63 evolution should be considered in the determination of saline intrusion length. Estuarine  
64 topographies reflected the influences of tidal amplitude and river flow, along with some  
65 representation of alluvium (Prandle and Lane, 2015). Topography change was caused by natural  
66 evolution over long time scales and anthropogenic activities, especially in recent decades (Shen  
67 et al., 2003; Zhu and Bao, 2016).

68 Changjiang, also known as the Yangtze River, is one of the largest rivers in the world. The  
69 river discharges large amounts of freshwater ( $9.24 \times 10^{11} \text{ m}^3$ ) into the East China Sea each year  
70 (Shen et al., 2003). The seasonal variation of river discharge ranges from a maximum monthly  
71 mean of  $49,850 \text{ m}^3\text{s}^{-1}$  in July to a minimum of  $11,180 \text{ m}^3\text{s}^{-1}$  in January (Zhu et al., 2015). The  
72 estuary has a 90-km-wide river mouth and a nearly 640-km tidal limit. The Changjiang Estuary  
73 is characterized by multiple bifurcations (Fig. 1). The estuary is first divided into the South

74 Branch (South Branch) and the North Branch (North Branch) by Chongming Island. The lower  
75 South Branch was then bifurcated into the South Channel (South Channel) and the North  
76 Channel (North Channel) by Changxing Island and Hengsha Island. The South Channel was  
77 again bifurcated into the South Passage and the North Passage by the Jiudian Sandbank. In 2017,  
78 the mean water depths in the North Branch, South Branch, North Channel, South Channel, and  
79 North and South Passages were 4.27, 10.41, 8.34, 11.47, 7.22 and 5.75 m, respectively. Tides in  
80 the Changjiang Estuary are semidiurnal, and fortnightly spring-neap signals and the most  
81 energetic source of water movement, which are close to a mesoscale. The maximum spring tide  
82 range was 3.38 m and the minimum neap tide range was 0.64 m at the Baozhen hydrological  
83 station (Fig. 1b) (Zhu, et al., 2015). The maximum tidal current amplitudes reached  
84 approximately 2.0 m/s at the river mouth during spring tide. The prevailing monsoon climate  
85 resulted in a stronger northerly wind of 5.5 m/s during winter and a southeasterly wind of 5.0 m/s  
86 during summer (Zhu, et al., 2015). The northerly wind produced a southward current along the  
87 Jiangsu coast in winter, which resulted in a higher water level along the coast by the Ekman  
88 transport. So the northerly wind caused a horizontal circulation around the Changjiang Estuary,  
89 which flowed into the estuary in the North Channel and out of the estuary in the South Channel  
90 (Wu et al., 2010; Li et al., 2012).

91 River discharge and tides are major control factors of saltwater intrusion in the Changjiang  
92 Estuary (Li et al., 2010; Qiu et al., 2012; Shen et al., 2003; Wu et al., 2006; Zhu et al., 2010;) but  
93 is also influenced by wind (Li et al., 2012), topography (Li, et al., 2014), anthropogenic activities  
94 in the river basin and estuary (Lyu and Zhu, 2018a; Qiu and Zhu, 2013; Zhu, et al., 2006) and  
95 sea-level rise (Qiu and Zhu, 2015). The North Branch is always found to be filled with highly  
96 saline water due to a low river discharge and high tidal range. In addition, saltwater intrusion is

97 found to be the strongest in the South Passage and the weakest in the North Channel, mainly in a  
98 landwards wedge-like manner, especially during neap tide, similar to those observed in other  
99 partially mixed estuaries (Shen et al., 2003). During the dry seasons, when the river discharge is  
100 low, the North Branch always contains highly saline water under strong tidal conditions and low  
101 river discharge. Due to the bifurcation nature of the estuary, there is a particular type of saltwater  
102 intrusion in Changjiang Estuary compared with the other estuaries in the world, which is known  
103 as saltwater spillover (SSO) from the North Branch into the South Branch, and the SSO  
104 commonly occurs during spring tides of the dry seasons (Shen et al., 2003; Wu et al., 2006; Wu  
105 and Zhu, 2007; Wu et al., 2010; Zhu et al., 2016), which are defined as the period from  
106 November to March (next year) when the river discharge is usually low. Only a small amount of  
107 the saltwater returns to the North Branch because the shoals in its upper reaches surface during  
108 ebb tides. The saline water from the SSO during spring tides is transported downstream by runoff  
109 during the subsequent middle tides and neap tides. This pattern of saltwater intrusion poses a  
110 significant threat to the security of freshwater resources stored in three reservoirs in the estuary:  
111 Qingcaosha Reservoir (QCSR), Chenhang Reservoir (CHR) and Dongfengxisha Reservoir  
112 (DFXSR) (Table 1). The capacity The QCSR is the largest among them and is located in the  
113 North Channel, along the northwestern coast of Changxing Island (shown in Fig. 1). The QCSR  
114 supplies more than 70% of the freshwater for city Shanghai. But the QCSR is frequently  
115 influenced by saltwater intrusion particularly during the dry seasons. The current regulations  
116 prevent these reservoirs from taking water from the Changjiang when the salinity is more than  
117 0.45 psu, to meet the standard for drinking water. For convenience of understanding the more  
118 acronyms in this paper, the acronyms and their corresponding full names were listed in the  
119 Appendix 1.

120 **Table 1**

121 The capacity, daily supply and their feeding population of three reservoirs.

Reservoir	Capacity ( $\times 10^4$ m <sup>3</sup> )	Daily supply ( $\times 10^4$ t/day)	Population ( $\times 10^4$ )
QCSR	52400	500	1300
CHR	956	130	300
DFXSR	976	15	82

122

123 Previous studies on the impacts of topography change on saltwater intrusion in the  
124 Changjiang Estuary include the works of Chen and Zhu (2014a) and Lyu and Zhu, 2018a. Li et  
125 al. (2014) calculated the differences in saltwater intrusion in the northern outlet of the North  
126 Channel in the Changjiang Estuary using different topographic data. Zhu and Bao (2016)  
127 calculated the evolution of saltwater intrusion in the Changjiang Estuary in 1950s, 1970s and  
128 2010s. Despite of those studies, the impacts of topography change on saltwater intrusion in the  
129 Changjiang Estuary in the recent years have received a little attention. The aim of this study is  
130 to bridge the knowledge gap and gain further understanding of the impacts of topography  
131 change on estuarine saltwater intrusion and provide a reference to explain similar phenomena in  
132 other estuaries.

133 To study estuarine saltwater intrusion, theoretical method is commonly used to obtain  
134 analytic solutions from simplified partial differential equations, i.e., the linear momentum  
135 equation of a dynamic balance between horizontal pressure gradient and vertical turbulent  
136 viscosity stress, equations for conservation of water and salt in steady state. There are many  
137 theoretical studies on the relation between the saltwater intrusion and stratification and vertical  
138 mixing in estuaries. For example, Ippen and Harleman (1961) demonstrated that vertical mixing  
139 could be related to energy considerations and defined a stratification number that is a ratio of  
140 energy dissipation to gain potential energy. Afterwards, Ippen (1966) modified the stratification

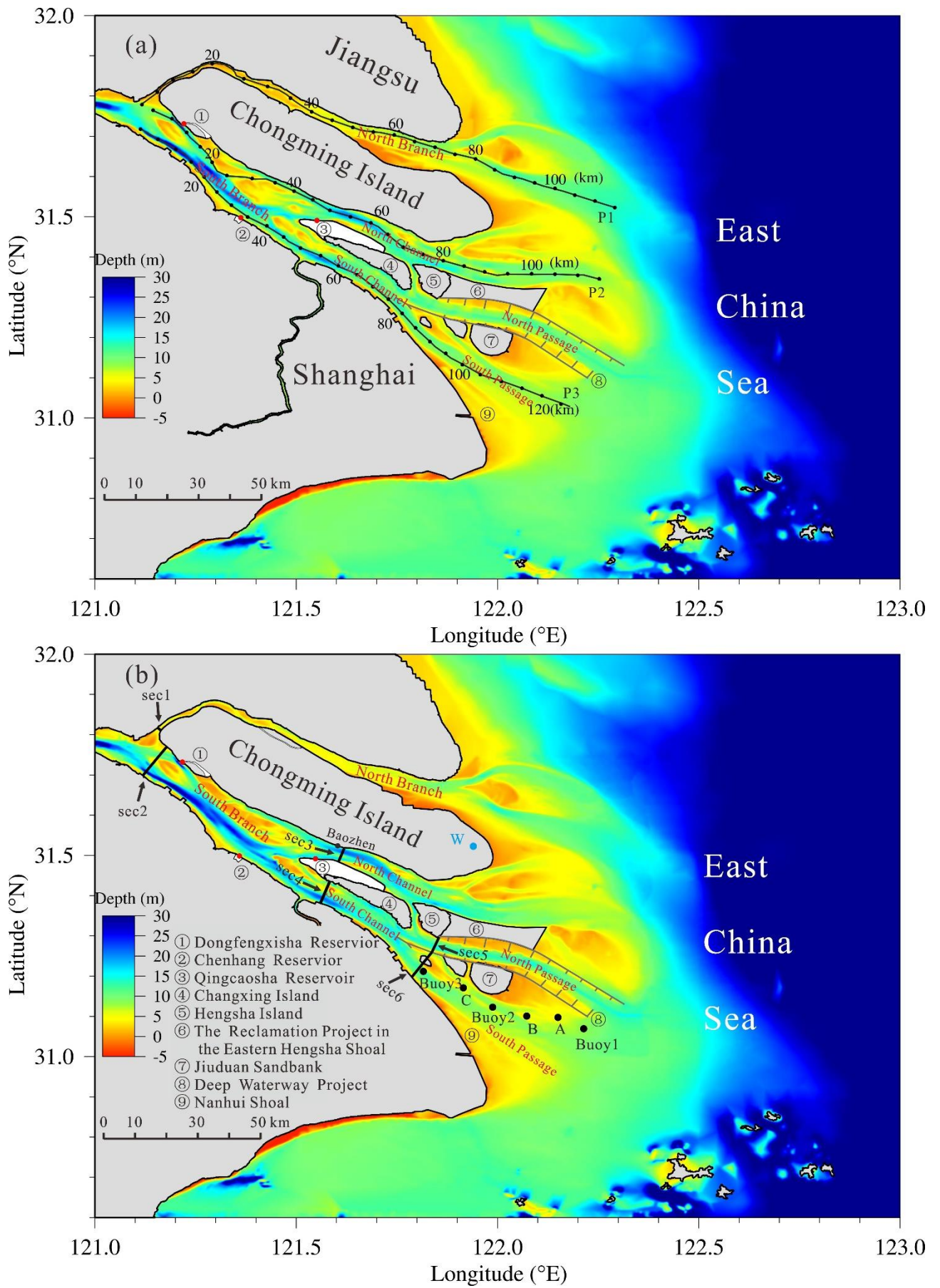
141 number of the available tidal energy (effective in mixing) to that required to mix river and  
142 seawater within the saline intrusion length, which is proportional to the square of the water depth.  
143 In the same year, Hansen and Rattray (1966) discussed the correlation between the vertical  
144 variations in mean velocity and salinity and the role of this correlation in maintaining the  
145 steady-state salinity distribution in estuaries where turbulent mixing results primarily from tidal  
146 currents. It indicated the variation of water depth would have significant impact on salinity  
147 vertical mixing in an estuary. Moreover, some theoretical studies showed that the variation of  
148 water depth would also affected the estuarine horizontal mixing. Ippen (1966) proposed the  
149 length of an arrested saline wedge based on residual velocity profiles for a stratified estuary,  
150 which is a function of water depth, residual velocity, difference in density between bed and  
151 surface, and a parameter that varies with river conditions. Prandle and Lane (2015) deduced an  
152 explicit expression for saline intrusion length, which shows the river mouth depth is proportional  
153 to the saline intrusion length. They also addressed the question of how tidally dominated  
154 estuaries would adapt to increases in mean sea level. It was concluded that a mean sea-level rise  
155 would have a significant impact in shallow microtidal estuaries.

156 Review of previous studies suggested that, the estuarine topography change would have a  
157 great influence on saltwater intrusion in the horizontal and vertical directions. Whilst the referred  
158 theoretical studies could quantify the change of saltwater intrusion in the single-channel estuaries,  
159 given that the Changjiang Estuary is a multi-bifurcated channel with complex topography and  
160 there exists the complicated SSO, it makes it much more difficult to obtain an analytic solution  
161 to reflect the real temporal and spatial variations in saltwater intrusion. Nonlinear interactions  
162 between the river discharge, tide, wind stress and topography should be included in investigating  
163 the complicated patterns of saltwater intrusion in the estuary. It therefore becomes necessary to

164 employ and advanced 3D numerical model with the capability of solving the primitive equations  
165 in this study to simulate the impacts of topography changes from 2007 to 2017 on saltwater  
166 intrusion and water resources and capture the variation of hydrodynamics from natural forcing  
167 and human activities during this period.

168 In the following sections, the topography changes from 2007 to 2017, and numerical  
169 model set up and validation are described, followed by the analysis and comparisons of the  
170 water and salt transport, water diversion ratio (WDR), and saltwater intrusion in the estuary.  
171 The saltwater intrusion is also predicted under in the scenario that the North Branch is  
172 completely silt-up and the conclusions are presented finally.

173



174

175

Fig. 1. The measured topographies of the Changjiang Estuary in 2007 (a) and 2017 (b), in

176 which: A, B and C are ship measurement sites; Buoys 1-3 are buoy measurement locations; Red  
177 dots are locations of water intakes of three reservoirs; sec1-sec6 and P1-P3 are cross-sectional  
178 longitudinal sections for saltwater intrusion analysis; and W is the location of the weather  
179 station.

## 180 **2. Methods**

### 181 **2.1 Topographic data**

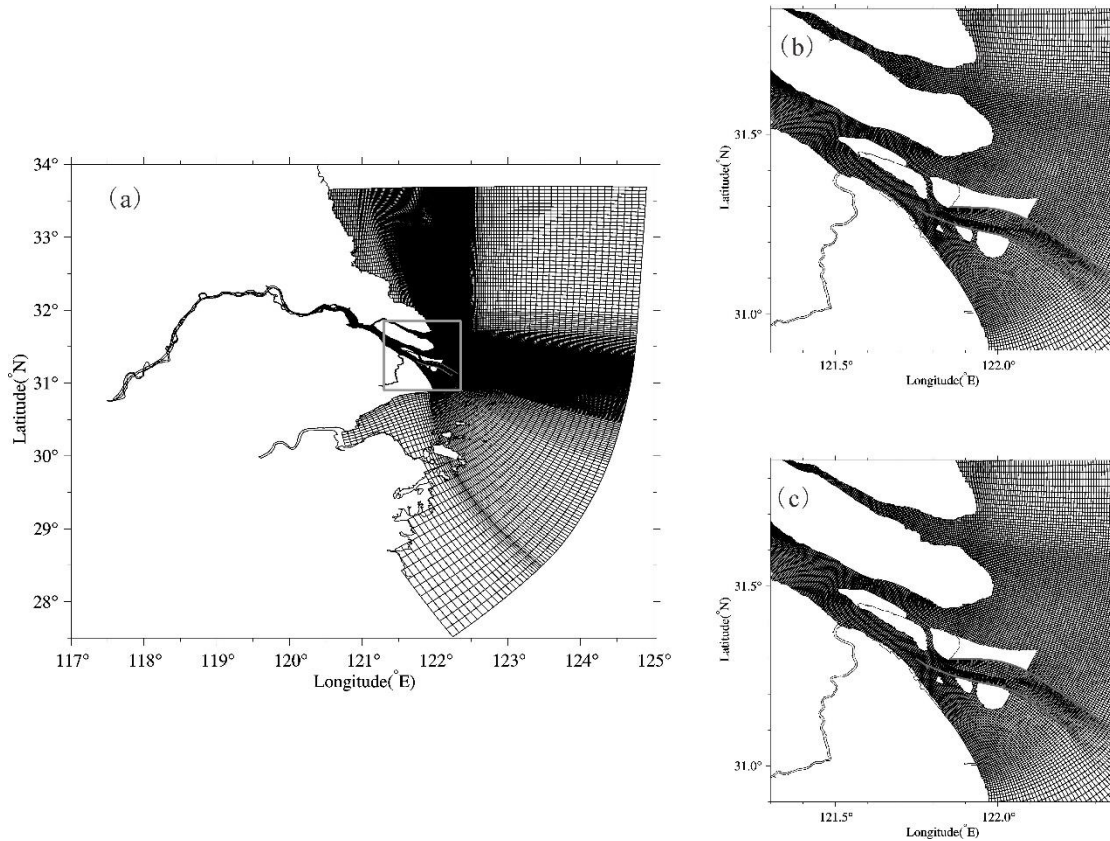
182 In this study, the topographic data as shown in Fig. 1, was sourced from the State Key  
183 Laboratory of Estuarine and Coastal Research, surveyed in 2007 and 2017 which reflect the  
184 changes in topography over that period.

### 185 **2.2 Model Setup**

186 To investigate the impacts of topography change on saltwater intrusion in the Changjiang  
187 Estuary over period from 2007 to 2017, a well calibrated 3D numerical model was used. The  
188 numerical model was based on ECOM-si (Blumberg 1994) and later improved by Chen et al.  
189 (2001) and Zhu (2003) for studying hydrodynamics and substance transport. The HSIMT-TVD  
190 (high-order spatial interpolation at the middle temporal level coupled with a total variation  
191 diminishing scheme limiter) of the advection scheme was developed to significantly reduce the  
192 numerical diffusions with third-order accuracy (Wu and Zhu, 2010). The Mellor-Yamada 2.5  
193 order turbulence closure module (Mellor and Yamada, 1982) with stability parameters from  
194 Kantha and Clayson (1994) was included. The model used a sigma coordinate system in the  
195 vertical direction and a curvilinear non-orthogonal grid in the horizontal direction (Chen et al.,  
196 2004). A wet/dry scheme was included to describe the intertidal area with a critical depth of 0.2  
197 m (Zheng et al., 2003; Zheng et al., 2004).

198 The computational domain of the model for this study covers the Changjiang Estuary and

199 its adjacent sea (Fig. 2), from 117.5°E to 124.9°E and from 33.7°N to 27.5°N. The model grid  
200 was composed of  $337 \times 225$  curvilinear cells horizontally and 10 uniform  $\sigma$  levels vertically. The  
201 minimal grid resolution reaches nearly 100 m in the bifurcation of the South Branch and North  
202 Branch to better simulate the SSO (Fig. 2). The resolution was relaxed to  $\sim 10$  km near the open  
203 boundary.



204  
205 **Fig. 2.** Numerical model grid (a) and the detailed model grid around the Changjiang Estuary in  
206 2007 (b) and 2017 (c)

207  
208 Along the open sea boundary of the model, the tide was specified with the 16 astronomical  
209 tidal constituents ( $M_2$ ,  $S_2$ ,  $N_2$ ,  $K_2$ ,  $K_1$ ,  $O_1$ ,  $P_1$ ,  $Q_1$ ,  $MU_2$ ,  $NU_2$ ,  $T_2$ ,  $L_2$ ,  $2N_2$ ,  $J_1$ ,  $M_1$ , and  $OO_1$ ),  
210 derived from the NaoTide dataset (<https://www.miz.nao.ac.jp/staffs/nao99/>). Monthly mean river  
211 discharge recorded at the Datong hydrologic station from 1950 to 2016 (Changjiang Water  
212 Resources Commission) was used in the model as the river boundary condition. Wind data, with

213 a resolution of  $0.25^{\circ} \times 0.25^{\circ}$ , were adopted based on the semi-monthly mean of 10 years  
214 (2007-2017) from the NCEP (National Centers for Environmental Prediction) with a resolution  
215 of  $0.25^{\circ} \times 0.25^{\circ}$  (<https://www.ncep.noaa.gov>).

216 For this study, two numerical experiments were conducted using the topographies measured  
217 in 2007 and 2017. However, the topography change trends of the past decade showed that the  
218 North Branch was heavily deposited and the channel became narrow (Fig.1 (a, b)). Therefore, an  
219 additional numerical experiment was conducted which made the North Branch complete silt-up  
220 on the basis of 2017 experiment. In this numerical experiment, the grids and topographies were  
221 same with the 2017 experiment but all wet grids in the North Branch were transformed into dry  
222 grids. Because the tide was just the oscillation of ocean waters under the influence of the  
223 attractive gravitational forces of the moon and the sun (Simm et al., 1996). So the differences of  
224 astronomical tides during dry season in different years were small. To make sure the tidal  
225 condition identical in three experiments, we selected the same simulation time. All model  
226 simulations covered the period from December 1, 2016 to February 28, 2017 which was the  
227 typical dry season. Because the model need 1-2 months to adjust the hydrodynamic and salinity  
228 to be stable. Therefore the model results in February were used to analyze and compare the  
229 impacts of the topography change over the past decade and the North Branch complete silt-up on  
230 residual water and salt transport, WDR, and saltwater intrusion. The monthly averaged river  
231 discharge since 1950 was  $13600 \text{ m}^3/\text{s}$ ,  $11100 \text{ m}^3/\text{s}$  and  $12000 \text{ m}^3/\text{s}$  in December, January and  
232 February (dry season), and  $36000 \text{ m}^3/\text{s}$ ,  $45000 \text{ m}^3/\text{s}$  and  $40000 \text{ m}^3/\text{s}$  in June, July and August  
233 (flood season), respectively. The river discharge in dry season is much lower than in flood season.  
234 The integrated time step was set to 30 s for all test cases.

235 To describe the water and salt transport, the residual unit width water flux (RUWF) and the

236 residual unit width salt flux (RUSF) are defined as follows.

$$237 \quad \bar{Q} = \int_{h1}^{h2} \bar{V} d\sigma \quad (1)$$

$$238 \quad RUWF = \frac{1}{T} \int_0^T \bar{Q} dt \quad (2)$$

$$239 \quad RUSF = \frac{1}{T} \int_0^T \bar{Q} s dt \quad (3)$$

240 where  $\bar{Q}$  is the instantaneous rate of water transport per unit width through a water column,  
 241  $\bar{V}$  is the current vector,  $h1$ ,  $h2$  is the lower and upper bound depth of a layer, and  $\sigma$  is the  
 242 depth of layer bound.  $T$  is the time period (which equals one or several tidal cycles; in this study,  
 243 it equals six semidiurnal tidal cycles) and is used as an averaging time window to remove the  
 244 tidal signals, and  $s$  is salinity.

245 Additionally, the residual transection water flux (NTWF) is determined to calculate the  
 246 WDR between channels (transection locations labeled in Fig. 1) as follows.

$$247 \quad NTWF = \frac{1}{T} \int_0^T \int_{-H(x,y)}^{\zeta} \int_0^L \vec{V}_n(x, y, z, t) dl dz dt \quad (4)$$

248 where  $T$  is the same as above,  $\zeta$  is the elevation,  $L$   $l$  is the width of the transect, and  
 249  $\vec{V}_n(x, y, z, t)$  is the velocity component that is vertical to the transect.

250 Similarly, the residual (net) transection salt flux (NTSF) is determined as follows.

$$251 \quad NTSF = \frac{1}{T} \int_0^T \int_{-H(x,y)}^{\zeta} \int_0^L s \vec{V}_n(x, y, z, t) dl dz dt \quad (5)$$

252 where  $s$  is salinity.

253

### 254 **2.3 Model Validation**

255 The model has been extensively calibrated, validated and applied in a number of previous  
 256 studies in the Changjiang Estuary, which have shown that the model can reproduce the

257 observed water level, current and salinity with high simulation accuracy (Li et al. 2012; Lyu  
 258 and Zhu, 2018b; Qiu, et al., 2015; Wu and Zhu 2010). In this study, we used the measured data  
 259 taken in the South Passage from 9th to 19th March 2018 (three ship sites and three buoy sites  
 260 shown in Fig. 1b) to further validate the model results.

261 The river discharge at the Datong Hydrological Station and wind data recorded by the  
 262 weather station located on the east of the Chongming Island (indicate by W in Fig. 1) were  
 263 adopted during the measured period to run the model. Three skill assessment indicators were  
 264 used to quantify the current and salinity validation: the correlation coefficient (CC), root mean  
 265 square error (RMSE), and skill score (SS). As follows,

$$266 \quad CC = \frac{\sum (X_{\text{mod}} - \bar{X}_{\text{mod}})(X_{\text{obs}} - \bar{X}_{\text{obs}})}{[\sum (X_{\text{mod}} - \bar{X}_{\text{mod}})^2 \sum (X_{\text{obs}} - \bar{X}_{\text{obs}})^2]^{1/2}} \quad (6)$$

$$267 \quad RMSE = \sqrt{\frac{\sum (X_{\text{mod}} - X_{\text{obs}})^2}{N}} \quad (7)$$

$$268 \quad SS = 1 - \frac{\sum |X_{\text{mod}} - X_{\text{obs}}|^2}{\sum (|X_{\text{mod}} - \bar{X}_{\text{obs}}| + |X_{\text{obs}} - \bar{X}_{\text{obs}}|)^2} \quad (8)$$

269 where  $X_{\text{mod}}$  is the modeled data,  $X_{\text{obs}}$  is the observed data, and  $\bar{X}$  is the mean value.  $SS$   
 270 is a statistical metric developed by Wilmott (1981) to describe the degree to which the observed  
 271 deviations from the observed mean correspond to the predicted derivations from the observed  
 272 mean. Perfect agreement between the model results and observations yields an  $SS$  of 1.0,  
 273 whereas complete disagreement yields a value of 0. Temporal variations in the observed and  
 274 modeled water velocities and salinities at ship-measured site B in the middle tide after neap tide  
 275 and buoy-measured Buoy 2 were selected and shown in Fig. 3 and 4, respectively.

276 The assessment indicator scores of water velocity were summarized in Table 2. The values  
 277 of  $CC$  at the six sites ranged from 0.63 to 0.93 in the surface layer and from 0.51 to 0.84 in the  
 278 bottom layer; the  $RMSE$  ranged from 0.23 to 0.35 cm/s in the surface layer and from 0.10 to

279 0.21 m/s in the bottom layer; and the SS ranged from 0.79 to 0.93 in the surface layer and from  
 280 0.71 to 0.90 in the bottom layer. The mean water velocity values of CC, RMSE and SS at the  
 281 surface and bottom layers at six sites were 0.77, 0.23 cm/s and 0.86, respectively.

282 The assessment indicator salinity scores were summarized in Table 3. The CC at the six  
 283 sites ranged from 0.71 to 0.92 in the surface layer and from 0.66 to 0.90 in the bottom layer; the  
 284 RMSE ranged from 0.36 to 2.49 in the surface layer and from 0.29 to 2.14 in the bottom layer;  
 285 and the SS ranged from 0.80 to 0.96 in the surface layer and from 0.80 to 0.95 in the bottom  
 286 layer. The mean salinity values of CC, RMSE and SS at the surface and bottom layers at the six  
 287 sites were 0.83, 1.60 and 0.90, respectively. The assessment indicators indicated that the level  
 288 of model performance reached a high standard.

289 **Table 2**

290 Values of CC, RMSE, and SS of the modeled and observed flow velocity at the surface and  
 291 bottom layers at the measurement sites.

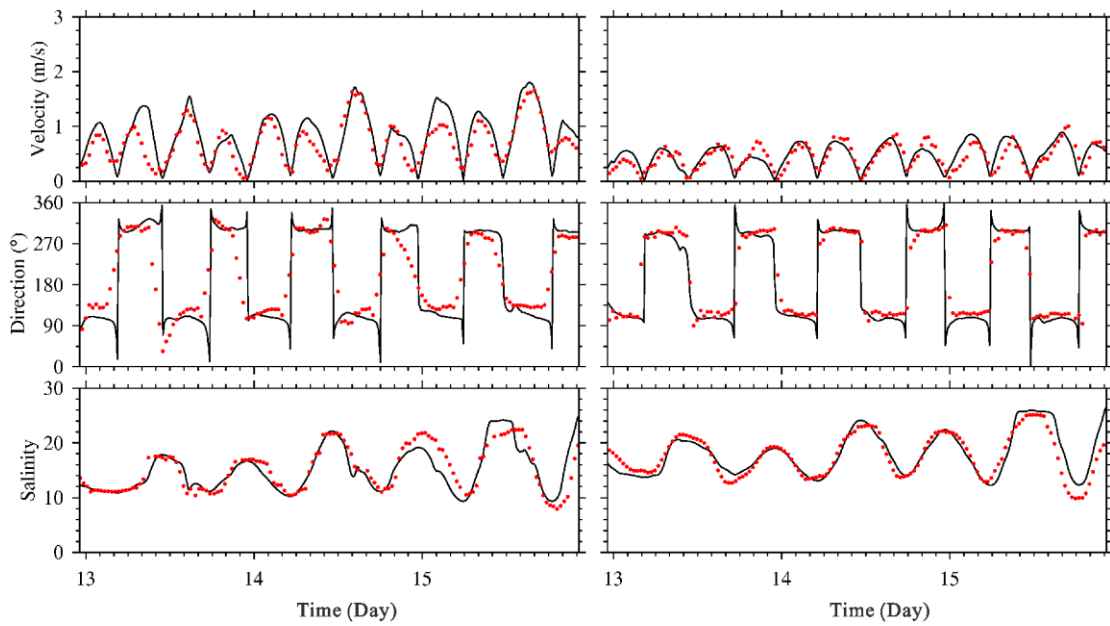
Layer	Sites	RMSE (m/s)	CC	SS
Surface	A	0.35	0.63	0.79
	B	0.23	0.93	0.89
	C	0.34	0.75	0.85
	Buoy 1	0.34	0.73	0.84
	Buoy 2	0.27	0.88	0.93
	Buoy 3	0.24	0.86	0.92
Bottom	A	0.21	0.51	0.71
	B	0.21	0.75	0.86
	C	0.18	0.73	0.84
	Buoy 1	0.11	0.78	0.87
	Buoy 2	0.12	0.84	0.90
	Buoy 3	0.10	0.80	0.88

292 **Table 3**

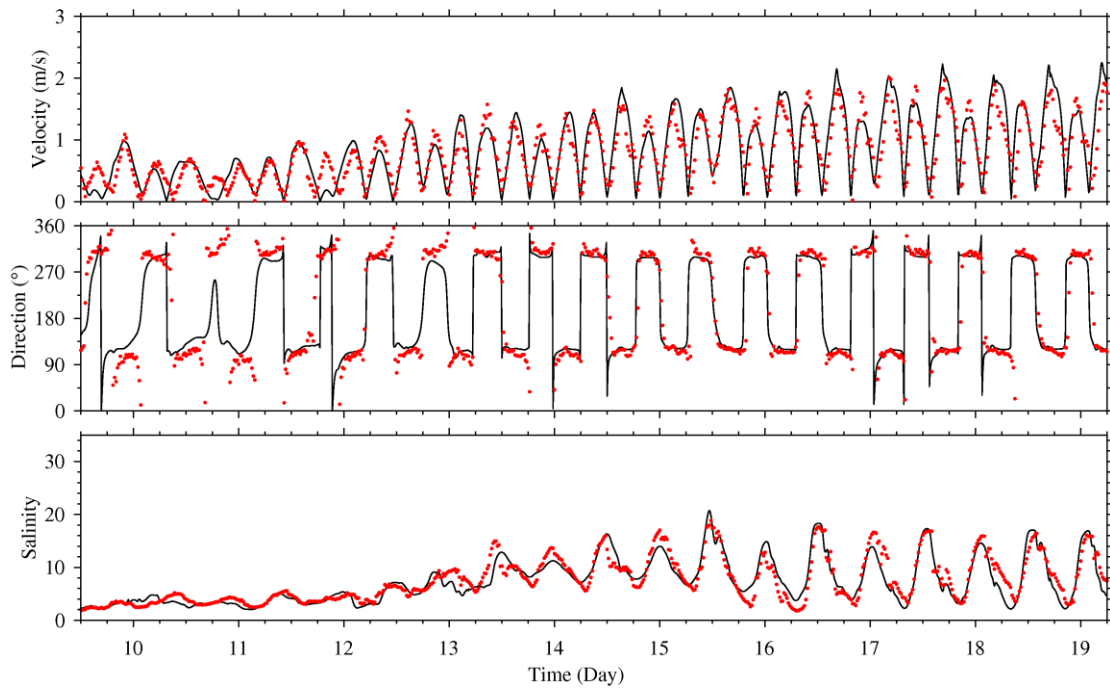
293 Values of CC, RMSE, and SS of the modeled and observed salinity at the surface and bottom  
 294 layers at the measurement sites.

Layer	Sites	RMSE	CC	SS
Surface	A	1.88	0.73	0.85
	B	2.49	0.85	0.90
	C	2.24	0.71	0.80
	Buoy 1	2.33	0.87	0.93
	Buoy 2	1.73	0.92	0.96
	Buoy 3	0.36	0.83	0.89
Bottom	A	2.14	0.66	0.80
	B	1.57	0.92	0.95
	C	1.30	0.86	0.92
	Buoy 1	1.31	0.87	0.92
	Buoy 2	/	/	/
	Buoy 3	0.29	0.90	0.95

295



296  
 297 **Fig. 3.** Comparisons of modeled (line) and measured (dots) flow velocity/direction and salinity  
 298 during neap tides at the surface layer (left panel) and bottom layer (right panel) at site B in  
 299 March 2018.



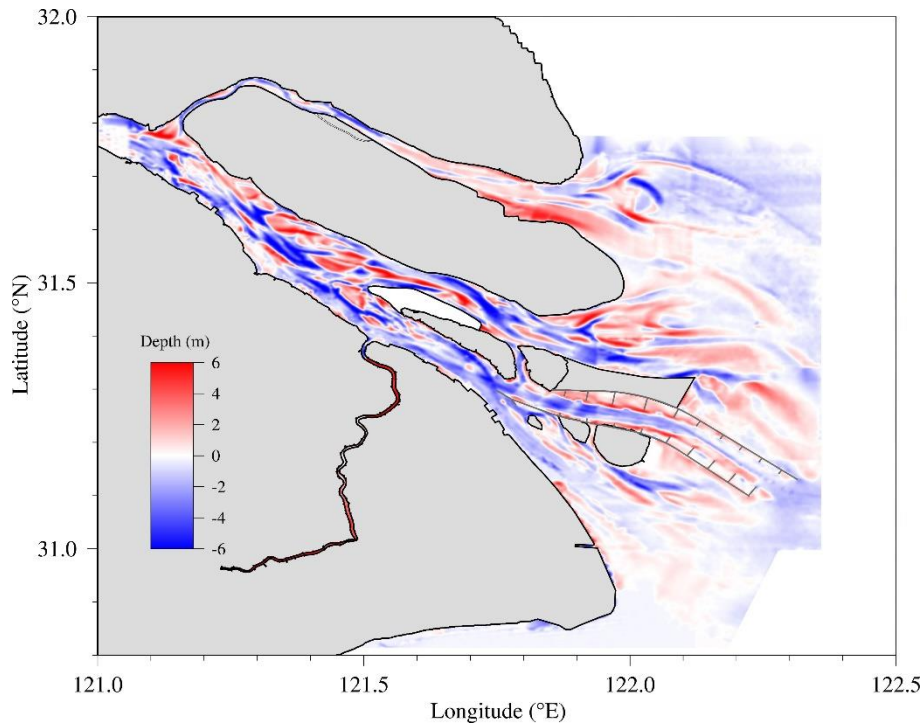
300  
 301 **Fig. 4.** Comparisons of modeled (line) and measured (dots) flow velocity/direction and salinity  
 302 at the surface layer at site Buoy 2 in March 2018.

303  
 304 **3. Results and Discussion**

### 305 **3.1 Topography change from 2007 to 2017**

306 During the period from 2007 to 2017, some major reclamation projects were conducted in  
307 the Changjiang Estuary, including the reclamation projects in the Eastern Hengsha Shoal, the  
308 Qingcaosha Reservoir (shown in Fig. 1b) for the demands of land and water. These projects  
309 considerably changed the local topography and further changed the topography in the entire  
310 estuary by altering the hydrodynamic processes (Lyu and Zhu, 2018a; Zhu and Bao, 2016). Due  
311 to these anthropogenic activities, the Changjiang Estuary has undergone dramatic topography  
312 change from 2007 to 2017. Fig. 1 showed the estuarine topographies for 2007 and 2017, while  
313 the topography change in the recent decade was shown in Fig. 5. The topography was found  
314 markedly changed in some places. The topography in the lower reaches of the North Branch was  
315 deposited approximately by 2 - 4 m overall. The area in the lower reaches of the North Branch  
316 and near Chongming Island has turned into land from the tidal flat, which made it narrower and  
317 shallower. In the South Branch, the area south of Chongming Island silted severely, and the  
318 maximum value reached a thickness of 6 m, while the middle of the channel deepened. In the  
319 North Channel, the depth north of the middle and lower QCSR was heavily deposited. In contrast,  
320 the depth deepened greatly south of Chongming Island and north of the middle QCSR, in the  
321 middle of the channel and east end of the QCSR. Near the mouth of the North Channel, the depth  
322 silted overall except the area north of Hengsha Island. The area east of the reclamation project of  
323 Eastern Hengsha Shoal silted 2-4 m. In the South Channel, the depth in the upper reaches  
324 deepened by 2-4 m. The depth became shallow north of the North Passage and became deep in  
325 the main channel in a range of approximately 2 m. The depth variation in the South Passage was  
326 smaller compared with other channels in a range of approximately 1 m. And the net volume  
327 change in the North Branch, South Branch, North Channel, South Channel, North and South

328 Passages were  $-1.73 \times 10^8$ ,  $3.24 \times 10^8$ ,  $9.34 \times 10^7$ ,  $2.90 \times 10^8$ ,  $-3.19 \times 10^7$  and  $1.03 \times 10^8$  m<sup>3</sup>,  
329 respectively (The negative indicates deposition). However, although the net volume changes in  
330 the North Channel indicated erosion as a whole, it was mainly eroded in the upper reaches. The  
331 lower reaches were significant deposition and net volume change in the lower reaches was  $-7.80$   
332  $\times 10^7$  m<sup>3</sup>.



333

334 **Fig. 5.** Topographic changes between 2007 and 2017 indicated by water depth changes  
335 measured in 2007 in 2017 (-ve = deposition and +ve= erosion).

336

### 337 3.2 RUWF, RUSE, Saltwater Intrusion and WDR in 2007

338 Fig. 6a shows that the surface RUWF flowed seaward in the South Branch, North and  
339 South Passages during the spring tide, but the RUWF flowed into the estuary in the North  
340 Branch due to its funnel shape and tidal Stokes transport (Qiu and Zhu, 2015). This indicated  
341 that the river runoff flows into the sea mainly through the North Channel, North and South  
342 Passages. In the upper reaches of the North Branch, the NTWF and WDR were  $-300.1$  m<sup>3</sup>/s and

343 -2.6% (Table 4), respectively, where the negative sign indicated that the water was transported  
344 from the North Branch into the South Branch. Most of the river runoff (72.8%) flowed into the  
345 sea through the North Channel compared with the South Channel (Table 5). Similarly, the South  
346 Passage was the main channel (54.3%) for the river runoff into the sea compared with the North  
347 Passage (Table 6). The RUWF flowed northward east of Chongming Island due to tidal  
348 pumping transport and tidal Stokes transport (Qiu and Zhu, 2015). Additionally, the RUWF in  
349 the South Branch was seaward in both the surface and bottom layers but smaller in the bottom  
350 layer due to bottom friction (Fig. 6b). Near the river mouth, the bottom RUWF was landward,  
351 which was believed to be induced by a strong salinity front (Pritchard, 1956). The RUWF  
352 flowed seaward in the surface layer and landward bottom layers east of the Eastern Hengsha  
353 Shoal. As shown in Fig. 6(c, d), the distribution of RUSF was similar to that of RUWF. Due to  
354 high salinity around the outside of the river mouth, the magnitude of the RUSF was much larger  
355 in that area. On the northern side of the North Passage, the RUSF flowed landward, which  
356 brought high salinity into the North Channel and the area east of Chongming Island. The North  
357 Branch was occupied by the highly saline water, and the SSO was simulated, which was caused  
358 by the RUWF and RUSF flowed into the South Branch from the North Branch in the upper  
359 reaches (Fig. 6). The less saline water northeastward extended east of Chongming Island, which  
360 corresponded to the RUSF. Obviously, the saltwater intrusion in the bottom was stronger.  
361 Among each outlet in the Changjiang Estuary, the saltwater intrusion was the weakest in the  
362 North Channel and strongest in the South Passage.

363 During neap tide (Fig. 7), around the area outside of the river mouth, the RUWF and RUSF  
364 flowed southward because the northerly winter monsoon effect was dominant with the tide  
365 becoming weaker (Wu et al., 2014). The SSO, which occurred during spring tide, disappeared.

366 The NTWF became positive (93 m<sup>3</sup>/s), and the WDR was 0.7% (Table 4). Compared with the  
 367 South Channel, the North Channel was the main channel for river discharge, which accounts for  
 368 66.7% (Table 5). Compared with the South Passage, more river runoff flowed into the sea from  
 369 the North Passage, accounting for 86.6% (Table 6), which was due to blocking of the stronger  
 370 salinity front in the South Passage. Near the river mouth, due to a strong horizontal salinity  
 371 gradient, the RUWF and RUSF in the bottom layer flow landward obviously. The saltwater  
 372 induced by the SSO during spring tide has arrived at the middle reaches of the South Branch.  
 373 Because the tidal mixing become weaker in neap tide than in spring tide, there existed distinct  
 374 saltwater wedges near the river mouth in neap tide, resulting in high stratification, i.e., the  
 375 bottom salinity was greater than the surface salinity.

376 **Table 4**

377 NTWF and WDR in the North and South Branches (NB and SB) during spring and neap tides in  
 378 2007 and 2017

Year	NTWF (m <sup>3</sup> /s)				WDR (%)			
	Spring		Neap		Spring		Neap	
	NB	SB	NB	SB	NB	SB	NB	SB
<b>2007</b>	-300.1	11804.9	93.4	12779.8	-2.6	102.6	0.7	99.3
<b>2017</b>	-330.9	11842.4	199.1	12606.8	-2.9	102.9	1.6	98.4
<b>Δ<sub>2017-2007</sub></b>	-30.8	37.5	105.7	-173.0	-0.3	0.3	0.9	-0.9

379

380

381

382 **Table 5**

383 NTWF and WDR in the North and South Channels (NC and SC) during spring and neap tides  
 384 in 2007 and 2017

Year	NTWF (m <sup>3</sup> /s)				WDR (%)			
	Spring		Neap		Spring		Neap	
	NC	SC	NC	SC	NC	SC	NC	SC
<b>2007</b>	8507.7	3180.4	8631.3	4303.8	72.8	27.2	66.7	33.3
<b>2017</b>	7655.1	4055.0	8060.2	4630.7	65.4	34.6	63.5	36.5
<b>Δ<sub>2017-2007</sub></b>	-852.6	874.6	-571.1	326.9	-7.4	7.4	-3.2	3.2

385

386 **Table 6**

387 NTWF and WDR in the North and South Passages (NP and SP) during spring and neap tides in  
 388 2007 and 2017.

Year	NTWF (m <sup>3</sup> /s)				WDR (%)			
	Spring		Neap		Spring		Neap	
	NP	SP	NP	SP	NP	SP	NP	SP
<b>2007</b>	2707.3	2282.2	5266.3	817.1	54.3	45.7	86.6	13.4
<b>2017</b>	3460.5	1750.9	5132.7	818.7	66.4	33.6	86.2	13.8
<b>Δ<sub>2017-2007</sub></b>	753.2	-531.3	-133.6	1.6	12.1	-12.1	-0.4	0.4

389

390

391

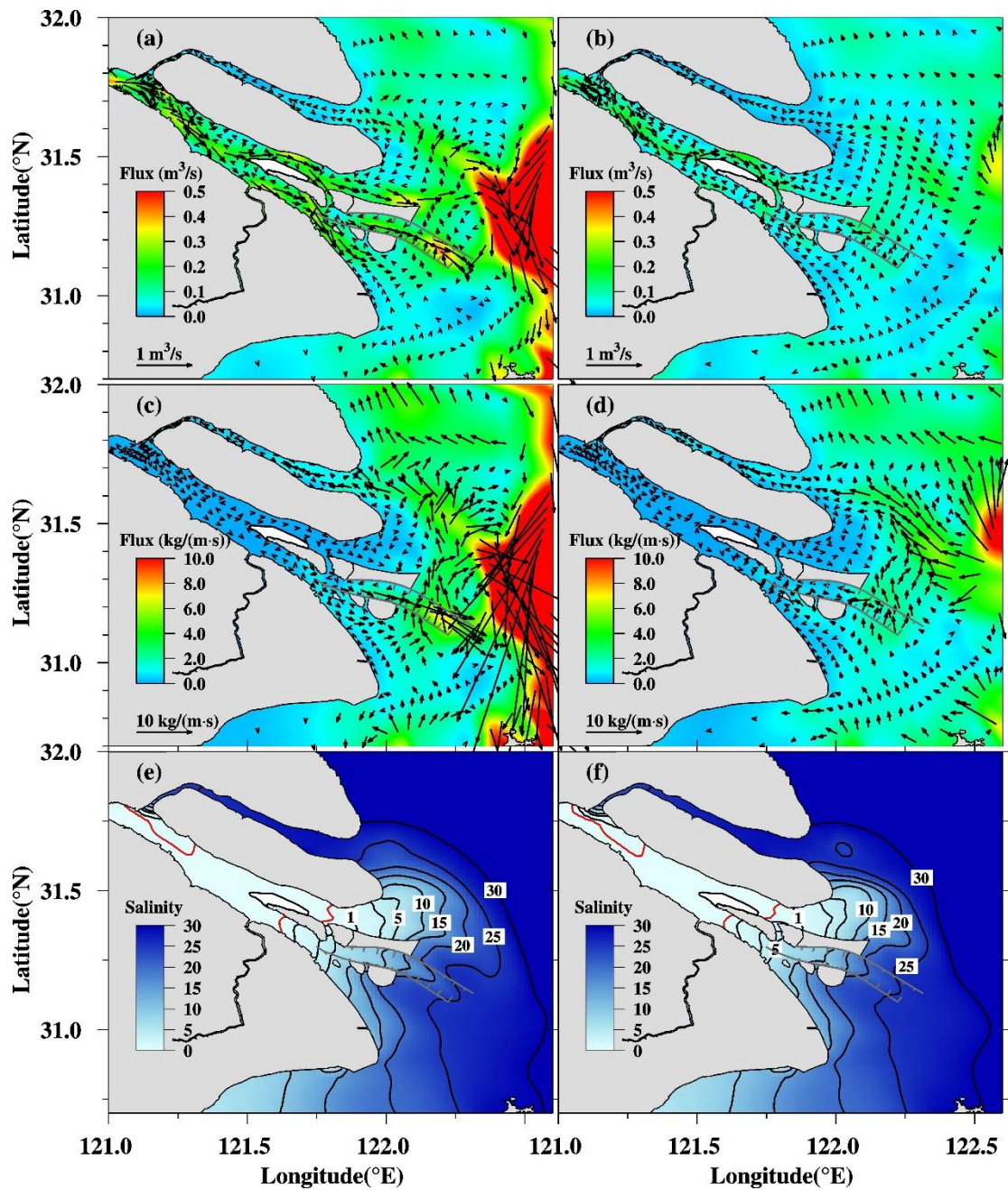
392 **Table 7**

393 NTSF in the North and South Branches (NB and SB) during spring and neap tides in 2007 and

394 2017

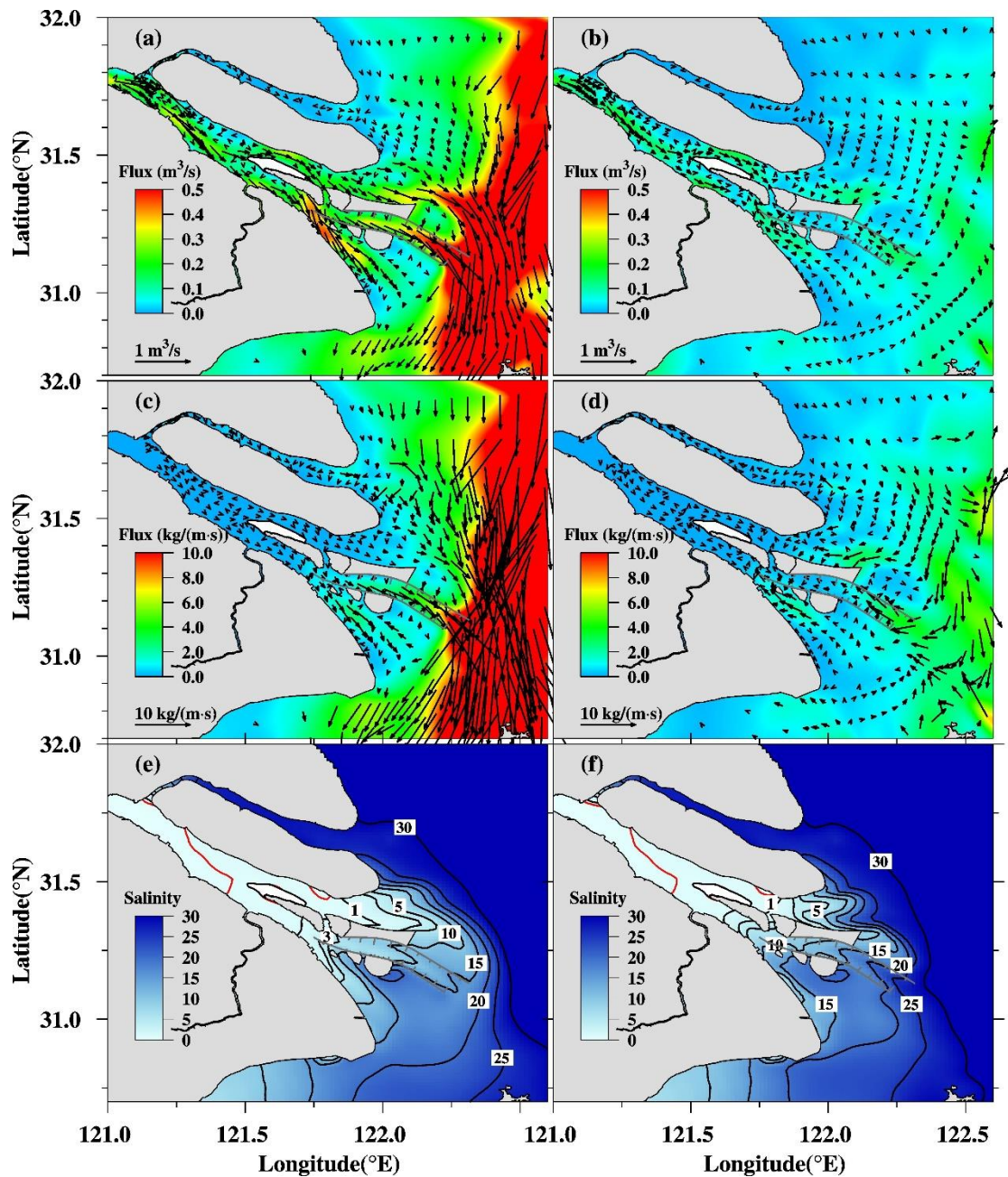
Year	NTSF (t/s)			
	Spring		Neap	
	NB	SB	NB	SB
<b>2007</b>	-7.70	7.45	0.03	0.12
<b>2017</b>	-6.10	5.81	0.04	0.12
<b><math>\Delta_{2017-2007}</math></b>	1.60	-1.64	0.01	0.00

395



396  
 397 **Fig. 6.** Distributions of RUWF (a, b), RUSF (c, d) and salinity (e, f) in the surface (left panel)  
 398 and bottom (right panel) layers during spring tides in 2007. (The red isohalines in (e, f) are 0.45,  
 399 the standard salinity for drinking water).

400



401

402 **Fig. 7.** Distributions of RUWF (a, b), RUSF (c, d) and salinity (e, f) in the surface (left panel)

403 and bottom (right panel) layers during neap tides in 2007.

404

405 **3.2 RUWF, RUSF, Saltwater Intrusion and WDR in 2017**

406 The differences in distributions of the RUWF, RUSF and salinity between 2017 and 2007

407 in the surface and bottom layers during spring tide were shown in Fig. 8. The differences of

408 RUWF and RUSF in the North Branch were landward, which was the same direction as RUWF

409 and RUSF in 2007, which meant that the saline transport from the sea to the North Branch  
410 increased in 2017. However, the salinity in the North Branch decreased overall as shown in Fig.  
411 8(e, f). This was because the topography became narrower and shallower in the middle and  
412 lower reaches of the North Branch (as shown in Fig. 1 and Fig. 5), which resulted in a decrease  
413 in the tidal volume. This could also cause the increase in the North Branch water velocity, so  
414 that the RUWF and RUSF increased. The NTWF in the North Branch was  $-330.9 \text{ m}^3/\text{s}$ , which  
415 increased by  $30.8 \text{ m}^3/\text{s}$  from the North Branch to the South Branch, but the NTSF decreased  $1.6$   
416  $\text{t/s}$  (Table 7). Therefore, the SSO became weaker overall in 2017 than in 2007. The salinity in  
417 the South Branch changed little. However, Fig.5 showed that major changes in topography were  
418 detected along the Southern Branch. It can be seen from Fig. 6(e, f) and Fig. 7(e, f) that the  
419 South Branch was almost occupied by freshwater because the South Branch is the main channel  
420 for river water discharging into the sea. Therefore, though major changes in topography were  
421 detected along the Southern Branch, the salinity was very low and its change was small.  
422 However, the topography changes in the South Branch could influence the water diversion  
423 ration in the North and South Branch, which could further influence the saltwater intrusion near  
424 the river mouth where there existed salinity front. A small change of water diversion ration can  
425 cause obvious isohaline move. That is why all the changes in isohaline were noticed near the  
426 mouth and further seaward. The difference of RUWF and RUSF in the North Channel was  
427 strongly correlated with that of the topography. The RUWF and RUSF increased with the  
428 increase of water depth. Fig. 8(e, f) show that the salinity in the North Channel increased,  
429 especially in the area east of Chongming Island and Eastern Hengsha Shoal, with a maximum  
430 value of more than 4.0. The deposition in these areas was noticeable (Fig. 5), which blocked the  
431 freshwater discharge into the North Channel. The WDR in the North Channel was 65.4% in

432 2017, which decreased by 7.4% compared with 2007 (Table 5), resulting in an overall increase  
 433 in salinity in the North Channel in 2017. Owing to the decrease in lower salinity water that  
 434 flowed over the area east of the Eastern Hengsha Shoal, the amount of lower saline water that  
 435 flowed cross the north dyke of the Deep Waterway to the south decreased under the action of  
 436 the north winter monsoon. Therefore, the salinity near the mouth of the North and South  
 437 Passages slightly increased.

438 During neap tide, the patterns of difference in the distributions of the RUWF, RUSF and  
 439 salinity between 2007 and 2017 in the surface and bottom layer were different from those  
 440 during spring tide, and the variations were the opposite in some areas (Fig. 9). In the North  
 441 Branch, the RUWF and RUSF showed little change with the weaker tide, while the WDR  
 442 increased in 2017, which caused the salinity in the North Branch to decrease overall. In the  
 443 South Branch, the difference in RUWF and RUSF was correlated with the difference in the  
 444 topography. Similar to that in the spring tide, the salinity east of Chongming Island and Eastern  
 445 Hengsha Shoal increased. However, the surface salinity near the 122.5°E area in the mouth of  
 446 the North Channel and the bottom salinity north of the Eastern Hengsha Shoal decreased by  
 447 more than 4.0 at its maximum. As shown in Fig. 9, the difference in the surface RUSF (Fig. 9c)  
 448 was the opposite of the surface RUSF (Fig. 7c) in 2007 near the 122.5°E area in the mouth of  
 449 the North Channel. This meant that the high salinity water from the north decreased. The  
 450 bottom salinity decreased because the saltwater wedge weakened. The salinity variation,  $s'$ , at  
 451 each layer and its mean value in the water column can be estimated with a polynomial  
 452 expression given by Hansen and Rattray (1966),

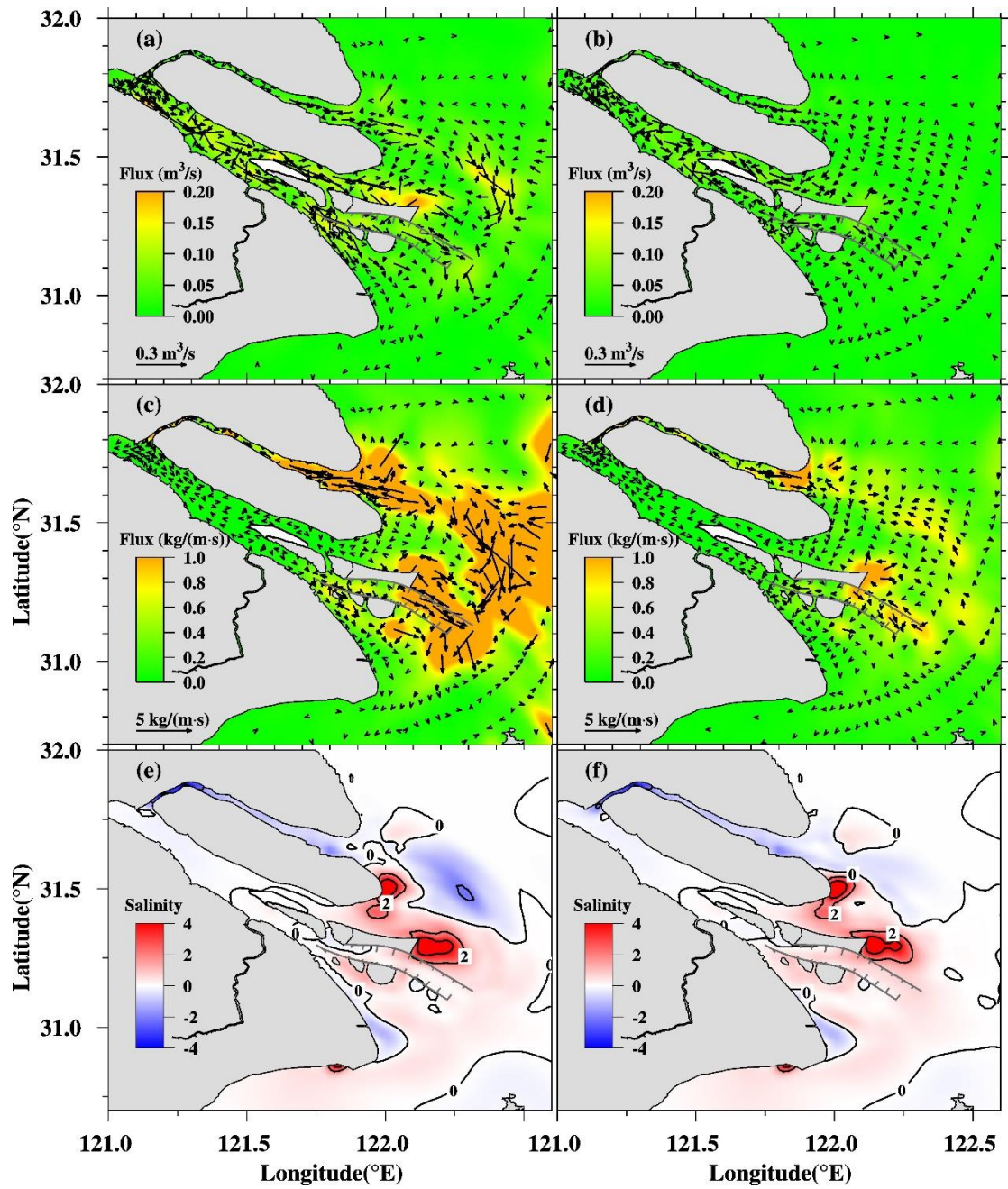
$$453 \quad s' = \frac{H^2}{K_S} \bar{s}_x [\bar{u}(-\frac{7}{120} + \frac{1}{4}\zeta^2 + \frac{1}{4}\zeta^2 - \frac{1}{8}\zeta^4) + u_E(-\frac{1}{12} + \frac{1}{2}\zeta^2 - \frac{3}{4}\zeta^4 - \frac{2}{5}\zeta^5)] \quad (6)$$

454 where  $\bar{s}$  indicates the width-averaged, tidally averaged salinity, which can be divided into  
 455 depth-average ( $\bar{s}$ ) and depth-varying ( $s'$ ) parts. The subscript  $x$  denotes the along-channel  
 456 partial derivative.  $K_s$  is the vertical eddy diffusivity; the dimensionless coordinate  $\zeta = z/H$ ,  
 457 where  $z$  indicates water depth, with  $z=0$  as the surface layer and  $z=-H$  as the bottom  
 458 layer, and  $H$  indicates topography. River discharge is given by  $\bar{u}$ ,  $u_E = g\beta\bar{s}_x H^3 / (48K_M)$ ,  
 459 where  $\beta \cong 7.7 \times 10^{-4} / PSU$  and  $K_M$  indicates the vertical eddy viscosity. When  $z=0$  and  
 460  $z=-H$ , formula (6) can be written as follows:

$$461 \quad \begin{cases} s' = -\frac{H^2}{120K_s} \bar{s}_x (7\bar{u} + 10u_E) & z = 0 \\ s' = \frac{H^2}{15K_s} \bar{s}_x (\bar{u} + u_E) & z = -H \end{cases} \quad (7)$$

462 It is clear that the increased  $H$  can augment the salinity variation  $s'$ . Therefore, as the  
 463 depth near the mouth of the North Channel was deposited all together (as shown in Fig. 5), the  
 464 decreased  $H$  reduced the variation  $s'$  near the bottom, resulting in a weaker gravitational  
 465 circulation that transported less oceanic saltwater into the estuary and decreased the bottom  
 466 salinity. Additionally, although the WDR in the North and South Passages had little variation,  
 467 namely, approximately 0.4%, the WDR in the South Channel increased by 3.2% in 2017,  
 468 resulting in a slight decrease in salinity.

469



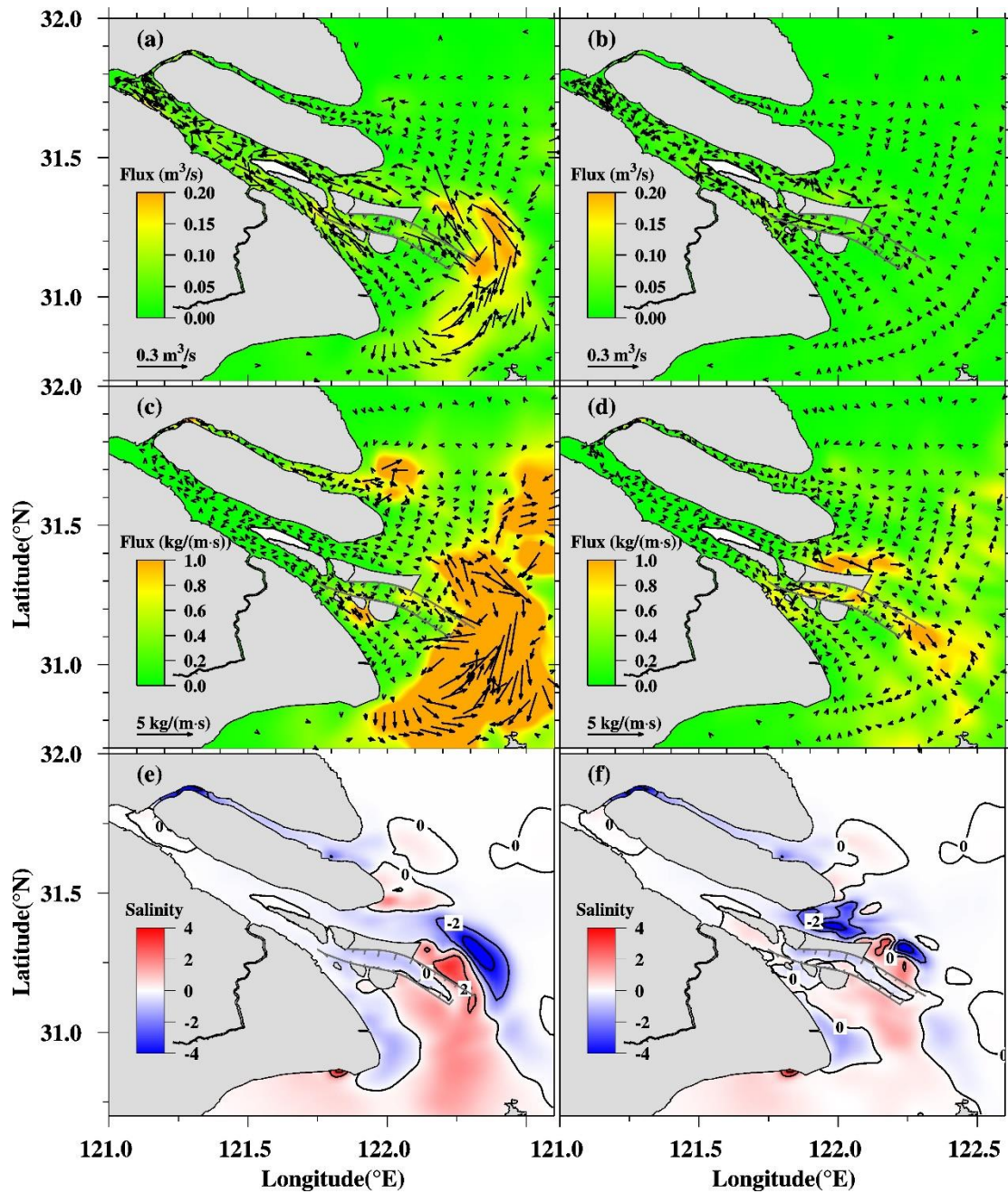
470

471 **Fig. 8.** Changes of RUWF (a, b), RUSF (c, d) and salinity (e, f) between 2017 and 2007 in the

472

surface (left panel) and bottom (right panel) layers during spring tides.

473



474

475 **Fig. 9.** Changes of RUWF (a, b), RUSF (c, d) and salinity (e, f) between 2017 and 2007 in the  
 476 surface (left panel) and bottom (right panel) layers during neap tides

477

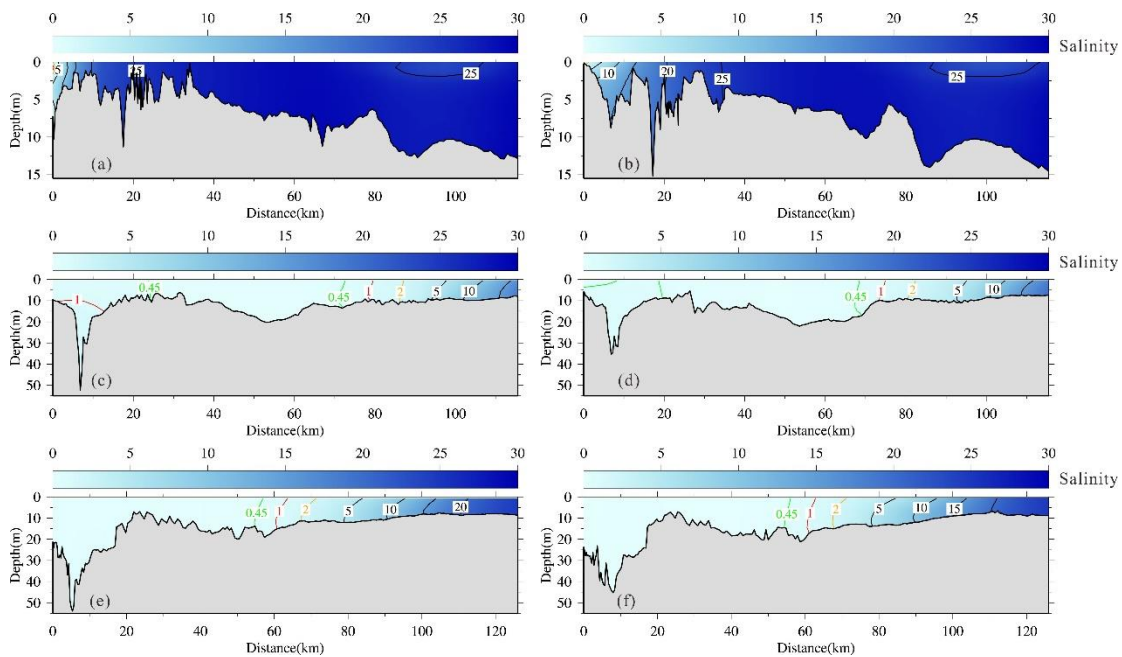
### 478 3.3 Variations in Vertical Salinity Distributions

479 The vertical distributions of salinity during spring tide along the North Branch profile (P1),  
 480 South Branch-North Channel profile (P2) and South Branch-South Passage profile (P3) in 2007  
 481 and 2017 are shown in Fig. 10. It was obvious that the depth near the bifurcation of the North

482 and South Branches became shallower. The depth at the start point of P1 was approximately 7.2  
483 m in 2007, but it became approximately 0.3 m in 2017. Although the depth at nearly 17.5 km  
484 increased from 11.5 to 15.2 m over the ten year period, the average depth from 40 to 80 km  
485 decreased from 7.3 to 6.62 m. Therefore, it would certainly decrease the tidal volume in the  
486 North Branch. In Fig. 10a, the isohaline was densely distributed between 0 and 20 km, and the  
487 bottom salinity was higher than the surface salinity. The isohaline distribution was sparser in  
488 2017, and the isohaline of 20 moved downstream from 10 km to 20 km. Overall, the saltwater  
489 intrusion in the North Branch became weaker in 2017 than in 2007. The vertical salinity  
490 distributions along P2 in 2007 and 2017 are shown in Fig. 10b. The water depth in 2017 became  
491 shallow overall. In the upstream and midstream areas, the depth changed slightly, except for the  
492 area near 7 km, which decreased from 52.4 to 35.4 m. The average depth in the downstream,  
493 namely, from 80 km to the end of P2, decreased from 9.9 to 9.1 m. The salinity in the upstream  
494 region was less than 0.45, indicating that freshwater existed. The intensity of SSO weakened in  
495 2017, which could be proven by the location of the bottom isohaline being 1 in 2007. Nearly all  
496 the isohalines in the downstream moved upstream by approximately 5 km in 2017 compared to  
497 2007. Therefore, the saltwater intrusion along the North Channel was enhanced in 2017. The  
498 vertical salinity distributions along P3 in 2007 and 2017 are shown in Fig. 10(e, f). The  
499 variation in depth was great at a distance of approximately 5 km from the start point of P3,  
500 which decreased from 53.9 to 41.8 m. Compared with the isohaline distribution in 2007, the  
501 variation was very small. In 2017, the isohalines moved upstream by approximately 1 km  
502 compared with that in 2007. The saltwater intrusion increased slightly in 2017.

503 During neap tide, the salinity upstream of the North Branch decreased markedly. In 2007,  
504 isohaline 0.45 appeared (Fig. 11a). Similar to that in the spring tide, the isohalines moved

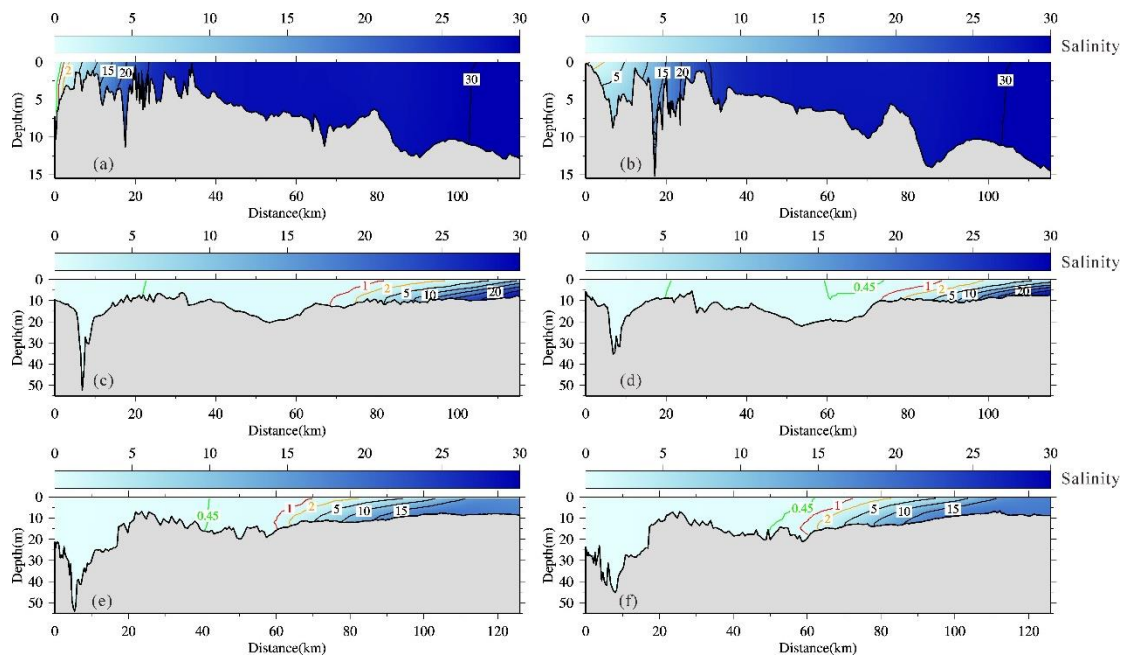
505 downstream by approximately 5 km in 2017. The saltwater intrusion in the North Branch was  
 506 also weakened in 2017. However, unlike during spring tide, the saltwater intrusion in the North  
 507 Channel became weaker in 2017 than that in 2007 because the main character of the saltwater  
 508 intrusion during neap tide was a salt wedge (Fig. 11b). Fig. 10c shows that the bottom salinity  
 509 was much greater than the surface salinity regardless of being in the North Channel or South  
 510 Passage. The average depth downstream was decreased from 9.9 m in 2007 to 9.1 m in 2017,  
 511 resulting in a reduction in bottom salinity. Isohaline 1 moved downstream by approximately 8  
 512 km in 2017, and isohaline 5 retreated from 82 km in 2007 to 88 km in 2017. Relative to the  
 513 North Channel, the depth in the South Passage showed little change. Because the WDR in the  
 514 South Channel increased from 33.3% to 36.5% over the last ten years, the saltwater intrusion  
 515 was weakened in 2017.



516

517 **Fig. 10.** Distribution of salinity along profiles P1(a, b), P2 (c, d) and P3 (e, f) during spring  
 518 tides in 2007 (left panel) and 2017 (right panel)

519



520

521

**Fig. 11.** Distribution of salinity along profiles P1(a, b), P2 (c, d) and P3 (e, f) during neap tides

522

in 2007 (left panel) and 2017 (right panel)

523

### 524 3.4 Scenario of Complete Silt-up of the North Branch

525

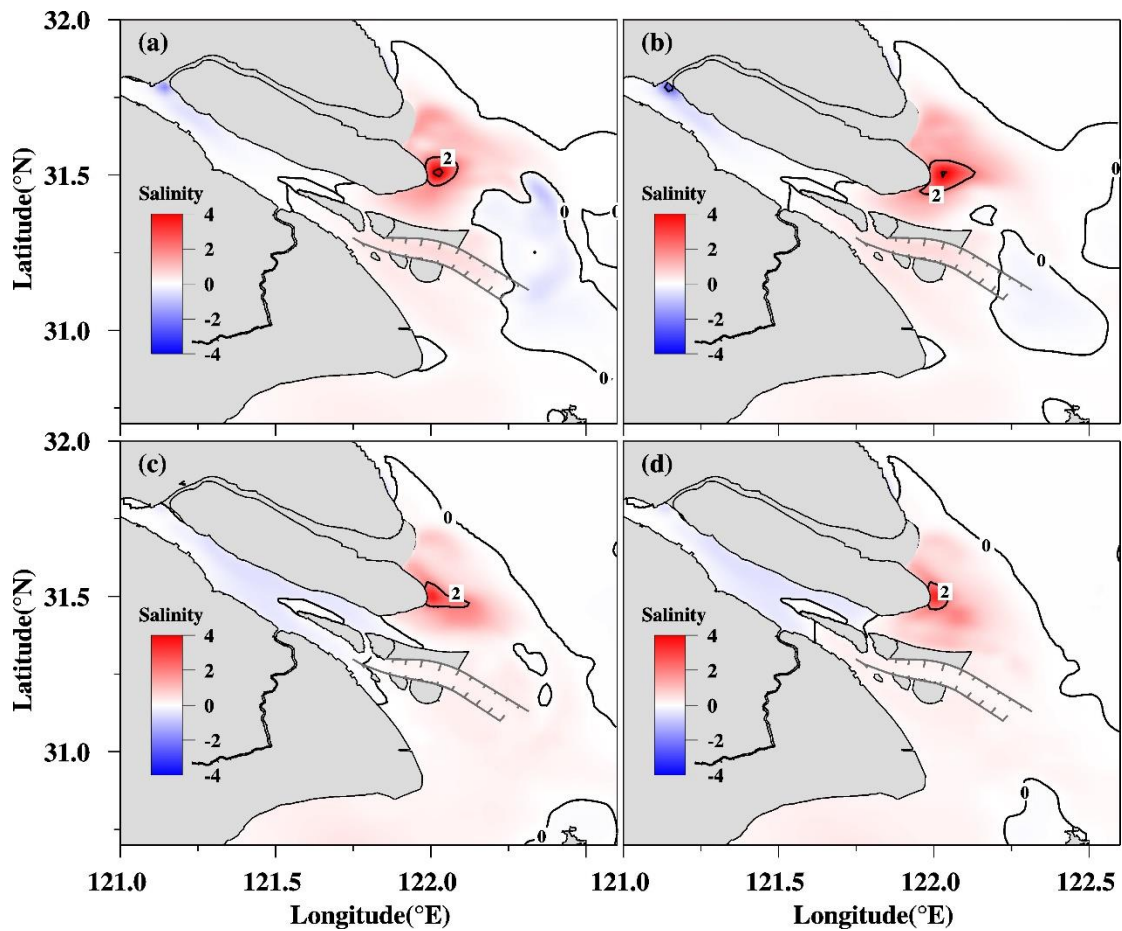
Over hundred years ago, the North Branch was the main channel discharging the river water into the sea and sediments were gradually deposited, especially since the 1960s, due to large tidal flat reclamation (Shen et al., 2003). Comparing the topography change in 2017 and 2007, the deposition at the upper entrance of the North Branch was very severe (Fig. 5). It is generally acknowledged that the North Branch will completely silt-up in the future. So we suppose the scenario that the North Branch would vanish and simulate its impact on saltwater intrusion and freshwater resources.

532

The SSO disappeared in the scenario of the North Branch silt-up, resulting in a salinity decrease in the South Branch. On the other hand, the river discharge was reduced in the North Channel, North and South Passages because there was no water spillover from the North Branch into the South Branch, which accounted for 2.9% of the total river discharge during the

535

536 spring tide in 2017 (Table 3), resulting in enhanced saltwater intrusion (Fig. 12). The salinity  
 537 decrease was at the upper reaches of the South Branch during spring tide and moved down to  
 538 the middle and lower reaches of the South Branch. Salinities at the water intakes of the three  
 539 reservoirs all decreased. The maximum salinity increase east of Chongming Island reached 2.  
 540 Therefore, vanishing of the North Branch weakened the saltwater intrusion in the South Branch  
 541 and enhanced it in the North Channel, North and South Passages.



542

543 **Fig. 12.** Changes in salinity between the scenario of complete silt-up in the North Branch and  
 544 2017 topography in the surface (left panel) and bottom (right panel) layers during spring tides  
 545 (a, b) and neap tide (c, d).

546

547 **3.5 Impacts on Water Resources**

548 The saltwater intrusion frequently threatens the freshwater intake from the Changjiang  
549 Estuary during winter due to low river discharge. Confirming the results of past studies, the  
550 salinities at the DFXSR and CHR were completely influenced by the SSO, but the QCSR was  
551 mainly impacted by the SSO and the saltwater intrusion along the North Channel (Chen and  
552 Zhu, 2014; Li and Zhu, 2018; Lyu and Zhu, 2018b).

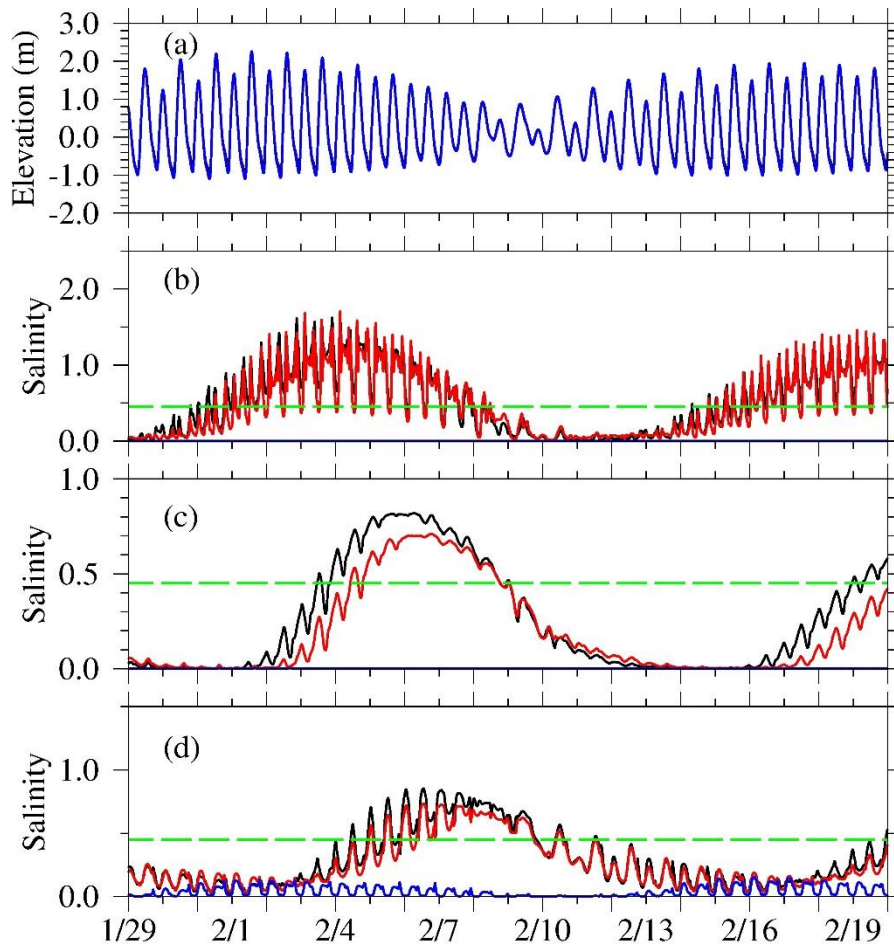
553 The temporal surface salinity variations and tidally averaged salinity in different tidal  
554 patterns (spring, middle tide after the spring tide (MTST), neap and middle tide after the neap  
555 tide (MTNT)) at the water intakes of the DFXSR, CHR and QCSR in 2007, in 2017 and in the  
556 scenario of vanishing of the North Branch are shown in Fig. 13 and Table 8, respectively. The  
557 temporal variations in the salinities showed that there were semidiurnal flood and ebb periods  
558 and semimonthly spring and neap period variations induced by tide. In 2007 and 2017, at the  
559 water intake of the DFXSR, the salinity was higher during the spring and MTST, and the  
560 salinity was lower during the neap and MTNT. The duration in which the salinity was lower  
561 than 0.45 was approximately half of the time in 2007 and 2017 in a complete neap-spring cycle,  
562 and the reservoir had enough time to take water from the Changjiang Estuary. In 2007, the  
563 tidally averaged salinity at the water intake of the DFXSR during spring tide, MTST, neap tide  
564 and MTNT were 0.80, 0.97, 0.16 and 0.08, respectively. At the water intake of the CHR, the  
565 duration in which the salinity was lower than 0.45, was greater than two-thirds of the time.  
566 Additionally, it took approximately 2.0 days for the saline water induced from the SSO flowed  
567 downstream to move from the water intake of the DFXSR to the water intake of the CHR,  
568 which we determined by comparing the salinity peak phase difference at the water intakes of  
569 the CHR and DFXSR (Fig. 13). In 2007, the tidally averaged salinity at the water intake of  
570 CHR during spring tide, MTST, neap tide and MTNT were 0.09, 0.74, 0.31 and 0.02,

571 respectively, meaning that water resources were optimistic in the CHR except during MTST. In  
572 2007, at the water intake of the QCSR, the duration in which the salinity was lower than 0.45  
573 was approximately half of the time. The tidally averaged salinity at the water intake of the CHR  
574 during spring tide, MTST, neap tide and MTNT were 0.10, 0.50, 0.53 and 0.22, respectively,  
575 meaning that water resources were optimistic in the QCSR except during MTST and neap tide.  
576 The above simulated temporal variation processes in salinity at the water intakes of three  
577 reservoirs were reasonably close to the published studies (Zhu et al., 2013; Zhu and Wu, 2013;  
578 Chen et al., 2019).

579 As mentioned above, the SSO were somewhat weakened after the last ten years, which  
580 resulted in the salinity being slightly decreased overall at the water intakes of the DFXSR, CHR  
581 and QCSR (Fig. 13). Owing to the saltwater sources were mainly from the SSO, the salinity  
582 was decreased by 0.17 and 0.06 at the water intake of the DFXSR during spring tide and MTST,  
583 and there were no changes during neap tide or MTNT. The salinity was decreased by 0.07 and  
584 0.16 at the water intake of the CHR during spring tide and MTST, and there was a slight  
585 increase of 0.02 during MTNT. The salinity decreased by 0.00, 0.09, 0.04 and 0.02 at the water  
586 intakes of the QCSR during spring tide, MTST, neap tide, and MTNT, respectively, which  
587 meant that the change in topography in the past ten years was favorable for the water resources  
588 of the three reservoirs in the Changjiang Estuary.

589 In the scenario of vanishing of the North Branch, the salinity approached 0 at the water  
590 intakes of the DFXSR and CHR and significantly decreased at the water intake of the QCSR  
591 due to vanishing of the SSO. The scenario of complete silt-up in the North Branch was greatly  
592 favorable for the utilization of freshwater resources in the Changjiang Estuary.

593



594

595

596

597

598

599

600 **Table 8**

601

602

**Fig. 13.** Time series of computed water levels at the water intake of the QCSR (a), surface salinity at the water intakes of the DFXSR (b), CHR (c) and QCSR (d) from January 29 to February 19. (Black lines: 2007 topography; red lines: 2017 topography; blue line: complete silt-up in the North Branch; green dashed line: the standard salinity of drinking water).

Averaged salinity over four tidal patterns at the water intakes of the DFXSR, CHR and QCSR in 2007 and 2017, the scenario of complete silt-up in the North Branch and in 2017

		Spring	MTST	Neap	MTNT
DFXSR	2007	0.80	0.97	0.16	0.08
	2017	0.63	0.91	0.16	0.08

	Scenario	0.00	0.00	0.00	0.00
	$\Delta_{2017-2007}$	-0.17	-0.06	0.00	0.00
	$\Delta_{\text{scenario-2017}}$	-0.63	-0.91	-0.16	-0.08
<hr/>					
CHR	2007	0.09	0.74	0.31	0.02
	2017	0.02	0.58	0.31	0.04
	Scenario	0.00	0.00	0.00	0.00
	$\Delta_{2017-2007}$	-0.07	-0.16	0.00	0.02
	$\Delta_{\text{scenario-2017}}$	-0.02	-0.58	-0.31	-0.04
<hr/>					
QCSR	2007	0.10	0.50	0.53	0.22
	2017	0.10	0.41	0.49	0.20
	Scenario	0.06	0.05	0.01	0.02
	$\Delta_{2017-2007}$	0.00	-0.09	-0.04	-0.02
	$\Delta_{\text{scenario-2017}}$	-0.04	-0.36	-0.48	-0.18
<hr/>					

603

#### 604 **4. Conclusions**

605 A well-validated 3D numerical model was used to simulate the impacts of topography  
606 change on saltwater intrusion over the past decade in the Changjiang Estuary. The residual  
607 water and salt transport, WDR and water resources with the topographies measured in 2007 and  
608 2017 in the Changjiang Estuary were analyzed. During the period from 2007 to 2017, the  
609 reclamation projects and the changing climate resulted in a considerable change in topography  
610 in the estuary. The model was validated with the data measured in the South Passage in March  
611 2018 and the results showed that the model produced satisfactorily the hydrodynamics and  
612 saltwater intrusion in the Changjiang Estuary.

613 The RUWF, RUSF, WDR and salinity distribution in 2007 and 2017 and the impacts of  
614 topography change in the last ten years were simulated and analyzed. Due to the topography  
615 change in the past ten years, the salinity decreased overall regardless of spring tide or neap tide  
616 in the North Branch, which was caused by the much shallower and narrower channel, resulting  
617 in a weaker SSO. In the North Channel, the salinity increased during spring tide, and the  
618 saltwater wedge weakened during neap tide due to a decrease in depth near the river mouth. The  
619 salinity increased slightly near the mouth of the North and South Passages during spring tide  
620 and decreased slightly in the upper reaches of the North and South Passages during neap tide.  
621 The changes in the saltwater intrusions in each channel were dynamically interpreted with the  
622 changes in RUWF, RUSF and WDR.

623 For the three reservoirs, there was about half time in a spring-neap period to take  
624 freshwater from the Changjiang Estuary into the reservoirs in the dry season of 2007 and 2017  
625 under mean river discharge. Because the saltwater intrusion in the North Branch and the SSO  
626 were weakened over the last ten years, the salinity at the water intakes of the DFXSR, CHR and  
627 QCSR decreased slightly, which was favorable for the fresh resources of the three reservoirs in  
628 the Changjiang Estuary.

629 In the scenario of complete silt-up in the North Branch, the SSO disappeared, and  
630 saltwater weakened in the South Branch, which was significantly favorable for the utilization of  
631 freshwater resources and enhances the North Channel, North and South Passages.

632 On the whole, influenced by the topography change in recent decade, saltwater intrusion  
633 weakened in the North Branch, enhanced in the North Channel, North and South Passages during  
634 spring tide and weakened during neap tide. Moreover, the results showed that the deposition or  
635 even complete silt-up in the North Branch was favorable for utilization of freshwater resources.

636 **Acknowledgements**

637 This work was partly supported by the National Natural Science Foundation of China  
638 (41676083), Shanghai Institute of Eco-Chongming and China Scholarship Council (CSC). The  
639 insightful suggestions from the anonymous reviewers are also acknowledged.

640

641 Appendix 1: A list of acronyms and their corresponding full names in the paper

---

---

Acronym	Full Name
SSO	Saltwater spillover
DFXSR	Dongfengxisha Reservoir
CHR	Chenhang Reservoir
QCSR	Qingcaosha Reservoir
NCEP	National Centers for Environmental Prediction
RUWF	Residual unit width water flux
RUSF	Residual unit width salt flux
NTSF	Net transection salt flux
NTWF	Net transection water flux
WDR	Water diversion ratio
CC	Correlation coefficient
RMSE	Root mean square error
SS	Skill score
MTNT	Middle tide after the neap tide
MTST	Middle tide after the spring tide

---

642

643 **References**

- 644 Blumberg, A.F., 1994. A primer for ECOM-si. Technical report of HydroQual, 66.
- 645 Chen, C.S., Zhu, J.R., Ralph, E., Green, S.A., Budd, J.W., Zhang, F.Y., 2001. Prognostic  
646 modeling studies of the Keweenaw current in Lake Superior. Part I: Formation and  
647 evolution. *Journal of Physical Oceanography*, 31 (2), 379-395.  
648 [https://dx.doi.org/10.1175/1520-0485\(2001\)031<0379:PMSOTK>2.0.CO;2](https://dx.doi.org/10.1175/1520-0485(2001)031<0379:PMSOTK>2.0.CO;2).
- 649 Chen, C.S., Zhu, J.R., Zheng, L.Y., Ralph, E., Budd, J.W., 2004. A non-orthogonal primitive  
650 equation coastal ocean circulation model: application to Lake Superior. *Journal of Great  
651 Lakes Research*, 30, 41-54. [https://doi.org/10.1016/S0380-1330\(04\)70376-7](https://doi.org/10.1016/S0380-1330(04)70376-7).
- 652 Chen, J., Zhu, J.R., 2014a. Impact of the reclamation project of Xincunsha on the saltwater  
653 intrusion in the North Branch of the Changjiang Estuary. *Journal of East China Normal  
654 University (Natural Science)*, 4, 163-172. [in Chinese with English abstract].
- 655 Chen, J., Zhu, J.R., 2014b. Sources for saltwater intrusion at the water intake of Qingcaosha  
656 Reservoir in the Changjiang Estuary. *Acta Oceanologica Sinica*, 36, 131-141.
- 657 Chen, Q., Zhu, J.R., Lyu, H.H., Chen, S.L., 2019. Determining Critical River Discharge as a  
658 Means to Provide Water Supply Security to the Changjiang River Estuary, China. *Journal  
659 of Coastal Research*, published online.  
660 <https://www.jcronline.org/doi/abs/10.2112/JCOASTRES-D-18-00165.1>
- 661 Geyer, W. R., 1993. The importance of suppression of turbulence by stratification on the  
662 estuarine turbidity maximum. *Estuaries and Coasts*, 16(1), 113-125.  
663 <https://dx.doi.org/10.2307/1352769>.
- 664 Hansen, D.V., Rattray J.M., 1966. Gravitational circulation in straits and estuaries. Technical  
665 Report No. 188, Department of Oceanography, University of Washington, Seattle,

666 Washington.

667 Ippen, A.T., 1966. Estuary and Coastline Hydrodynamics. McGraw-Hill, New York, NY, USA,  
668 ISBN 978 00 7032 015 4, p.744.

669 Ippen, A.T., Harleman, D.R.F., 1961. One-dimensional analysis of salinity intrusion in  
670 estuaries. Technical Bulletin no. 5, Committee on Tidal Hydraulics Waterways Experiment  
671 Station, Vicksburg, Mississippi.

672 Kantha, L.H., Clayson, C.A., 1994. An improved mixed layer model for geophysical  
673 applications. Journal of Geophysical Research Oceans, 99 (C12), 25235–25266.  
674 <https://dx.doi.org/10.1029/94JC02257>.

675 Li, G.P., Zhu, J.R., 2018. Analyses of saltwater intrusion at the water intake of qingcaosha  
676 reservoir in the changjiang estuary in dry season from 2015 to 2017. Journal of East China  
677 Normal University. 2, 160-169. [in Chinese with English abstract].

678 Li, L., Zhu, J.R., Wu, H., 2012. Impacts of wind stress on saltwater intrusion in the Yangtze  
679 Estuary. Science China Earth Sciences, 55 (7), 1178-1192.  
680 <https://dx.doi.org/10.1007/s11430-011-4311-1>.

681 Li, L., Zhu, J.R., Wu, H., Guo, Z.G., 2014. Lateral saltwater intrusion in the North Channel of  
682 the Changjiang Estuary. Estuaries and coasts, 37 (1), 36-55.  
683 <https://dx.doi.org/10.1007/s12237-013-9669-1>.

684 Li, L., Zhu, J.R., Wu, H., Wang, B., 2010. A numerical study on water diversion ratio of the  
685 Changjiang (Yangtze) estuary in dry season. Chinese Journal of Oceanology and  
686 Limnology, 28 (3), 700-712. <https://dx.doi.org/10.1007/s00343-010-9114-2>.

687 Lyu, H.H., Zhu, J.R., 2018a. Impacts of Tidal Flat Reclamation on Saltwater Intrusion and  
688 Freshwater Resources in the Changjiang Estuary. Journal of Coastal Research, 35(2),

689 314-321. <https://jstor.org/stable/26626840>.

690 Lyu, H.H., Zhu, J.R., 2018b. Impact of the bottom drag coefficient on saltwater intrusion in the  
691 extremely shallow estuary. *Journal of Hydrology*, 557, 838-850.  
692 <https://doi.org/10.1016/j.jhydrol.2018.01.010>.

693 Mellor, G.L., Yamada, T., 1982. Development of a turbulence closure model for geophysical  
694 fluid problems. *Reviews of Geophysics*, 20 (4), 851-875.  
695 <https://doi.org/10.1029/RG020i004p00851>.

696 Prandle, D., 1985. On salinity regimes and the vertical structure of residual flows in narrow  
697 tidal estuaries. *Estuarine, Coastal and Shelf Science*, 20(5), 615-635.  
698 [https://dx.doi.org/10.1016/0272-7714\(85\)90111-8](https://dx.doi.org/10.1016/0272-7714(85)90111-8).

699 Prandle, D., 2006. Dynamical controls on estuarine bathymetry: assessment against UK  
700 database. *Estuar. Coast. Shelf Sci.* 68 (1-2), 282-288.  
701 <https://dx.doi.org/10.1016/j.ecss.2006.02.009>.

702 Prandle, D., Lane, A., 2015. Sensitivity of estuaries to sea level rise: Vulnerability  
703 indices. *Estuarine, Coastal and Shelf Science*, 160, 60-68.  
704 <https://dx.doi.org/10.1016/j.ecss.2015.04.001>.

705 Pritchard, D.W., 1956. The dynamic structure of a coastal plain estuary. *J Marine Res*, 33-42.

706 Qiu, C., Zhu, J.R., 2013. Influence of seasonal runoff regulation by the Three Gorges Reservoir  
707 on saltwater intrusion in the Changjiang River Estuary. *Continental Shelf Research*, 71,  
708 16-26. <https://dx.doi.org/10.1016/j.csr.2013.09.024>.

709 Qiu, C., Zhu, J.R., 2015. Assessing the influence of sea level rise on salt transport processes and  
710 estuarine circulation in the Changjiang River estuary. *Journal of Coastal Research*, 31 (3),  
711 661-670. <https://www.bioone.org/doi/abs/10.2112/JCOASTRES-D-13-00138.1>.

712 Qiu, C., Zhu, J.R., Gu, Y.L., 2012. Impact of seasonal tide variation on saltwater intrusion in the  
713 Changjiang River estuary. *Chinese Journal of Oceanology and Limnology*, 30 (2), 342-351.  
714 <https://dx.doi.org/10.1007/s00343-012-1115-x>.

715 Shen, H.T., Mao, Z.C., Zhu, J.R., 2003. Saltwater intrusion in the Changjiang Estuary. Beijing:  
716 China Ocean. [in Chinese with English abstract].

717 Simm, J.D., Beech, N.W., John, S., 1996. A manual for beach management. In *Coastal*  
718 *Management: Putting Policy Into Practice: Proceedings of the Conference Organized by*  
719 *the Institution of Civil Engineers and Held in Bournemouth on 12-14 November 1995* (p.  
720 229). Thomas Telford.

721 Simpson, J.H., Brown, J., Matthews, J., Allen, G., 1990. Tidal straining, density currents, and  
722 stirring in the control of estuarine stratification. *Estuaries*, 13(2), 125-132.  
723 <https://dx.doi.org/10.2307/1351581>.

724 Simpson, J.H., Hunter, J.R., 1974. Fronts in the Irish Sea. *Nature* 250, 404-406.

725 Willmott, C. J., 1981. On the validation of models. *Physical geography*, 2(2), 184-194.  
726 <https://dx.doi.org/10.1080/02723646.1981.10642213>.

727 Wu, H., Shen, J., Zhu, J.R., Zhang, J., Li, L., 2014. Characteristics of the Changjiang plume and  
728 its extension along the Jiangsu Coast. *Continental Shelf Research*, 76(2), 108-123.  
729 <https://doi.org/10.1016/j.csr.2014.01.007>.

730 Wu, H., Zhu, J.R., 2007. Analysis of the transport mechanism of the saltwater spilling over  
731 from the North Branch in the Changjiang Estuary in China. *Acta Oceanologica Sinica*, (1),  
732 17-25. [in Chinese with English abstract].

733 Wu, H., Zhu, J.R., 2010. Advection scheme with 3rd high-order spatial interpolation at the  
734 middle temporal level and its application to saltwater intrusion in the Changjiang Estuary.

735 Ocean Modelling, 33 (1), 33-51. <https://dx.doi.org/10.1016/j.ocemod.2009.12.001>.

736 Wu, H., Zhu, J.R., Chen, B.R., Chen, Y.Z., 2006. Quantitative relationship of runoff and tide to  
737 saltwater spilling over from the North Branch in the Changjiang Estuary: A numerical  
738 study. Estuarine Coastal Shelf Science, 69 (1-2), 125-132.  
739 <https://dx.doi.org/10.1016/j.ecss.2006.04.009>.

740 Wu, H., Zhu, J.R., Choi, B. H., 2010. Links between saltwater intrusion and subtidal circulation  
741 in the Changjiang Estuary: a model-guided study. Continental Shelf Research, 30 (17),  
742 1891-1905. <https://dx.doi.org/10.1016/j.csr.2010.09.001>.

743 Zheng, L.Y., Chen, C.S., Liu, H.D., 2003. A modeling study of the Satilla River Estuary,  
744 Georgia. I: Flooding-drying process and water exchange over the salt marsh-estuary-shelf  
745 complex. Estuaries, 26 (3), 651-669. <https://doi.org/10.1007/BF02711977>.

746 Zheng, L.Y., Chen, C.S., Zhang, F.Y., 2004. Development of water quality model in the Satilla  
747 River Estuary, Georgia. Ecological modelling, 178 (3-4), 457-482.  
748 <https://doi.org/10.1016/j.ecolmodel.2004.01.016>.

749 Zhu, J.R., 2003. Ocean numerical calculation method and numerical model. Beijing: China  
750 Ocean Press. [in Chinese with English abstract].

751 Zhu, J.R., Bao, D.Y., 2016. The effects of river regime changes in the Changjiang Estuary on  
752 hydrodynamics and salinity intrusion in the past 60 years I. River regime changes.  
753 Haiyang Xuebao, 38 (12), 11-22. <https://doi.org/10.3969/j.issn.0253-4193.2016.12.0012>.

754 Zhu, J.R., Ding, P.X., Zhang, L.Q., Wu, H., Cao, H.J., 2006. Influence of the deep waterway  
755 project on the Changjiang Estuary. In The environment in Asia Pacific harbours (pp.  
756 79-92). Springer Netherlands. [https://dx.doi.org/10.1007/1-4020-3655-8\\_6](https://dx.doi.org/10.1007/1-4020-3655-8_6).

757 Zhu, J.R., Gu, Y.L., Wu, H., 2013. Determination of the period not suitable for taking domestic

758 water supply to the Qingcaosha Reservoir near Changjiang River Estuary. *Oceanologia et*  
759 *Limnologia Sinica*, 44(5), 1138-1145. [in Chinese with English abstract].

760 Zhu, J.R., Wu, H., 2013. Numerical simulation of the longest continuous days unsuitable for  
761 water intake in the Dongfengxisha Reservoir of the Changjiang Estuary. *Journal of East*  
762 *China Normal University (Natural Science)*, 5, 1-8. [in Chinese with English abstract].

763 Zhu, J.R., Wu, H., Li, L., 2015. Hydrodynamics of the Changjiang Estuary and Adjacent Seas.  
764 In *Ecological Continuum from the Changjiang (Yangtze River) Watersheds to the East*  
765 *China Sea Continental Margin* (pp. 19-45). Springer International Publishing.  
766 [https://dx.doi.org/10.1007/978-3-319-16339-0\\_2](https://dx.doi.org/10.1007/978-3-319-16339-0_2).

767 Zhu, J.R., Wu, H., Li, L., Wang, B., 2010. Saltwater intrusion in the Changjiang Estuary in the  
768 extremely drought hydrological year 2006. *Journal of East China Normal University*  
769 *(Natural Science)*, 4 (1), 1-6. [in Chinese with English abstract].